

RESEARCH FINAL REPORT

FLORIDA DEPARTMENT OF TRANSPORTATION

Project Title: Feasibility of atomic and molecular laser induced breakdown spectroscopy (LIBS) to *in situ* determination of chlorine in concrete

FDOT AGREEMENT # BDV31-977-32

FDOT CONTRACT # 00119410

UNIVERSITY OF FLORIDA – DEPARTMENT OF CHEMISTRY

PRINCIPAL INVESTIGATOR: NICOLÓ OMENETTO
omenetto@chem.ufl.edu
(352) 392-9853

PROJECT MANAGER: PAUL VINIK (FDOT)
Paul.Vinik@dot.state.fl.us
(352) 955-6686

Submitted September 2016

DISCLAIMER

The opinions, findings, and conclusions expressed in this publication are those of the authors and not necessarily those of the State of Florida Department of Transportation.

Approximate Conversions to SI Units

Symbol	When You Know	Multiply By	To Find	Symbol
Length				
in	inches	25.4	millimeters	mm
ft	feet	0.305	meters	m
yd	yards	0.914	meters	m
mi	miles	1.61	kilometers	km
Area				
in²	square inches	645.2	square millimeters	mm ²
ft²	square feet	0.093	square meters	m ²
yd²	square yard	0.836	square meters	m ²
ac	acres	0.405	hectares	ha
mi²	square miles	2.59	square kilometers	km ²
Volume				
fl oz	fluid ounces	29.57	milliliters	mL
gal	gallons	3.785	liters	L
ft³	cubic feet	0.028	cubic meters	m ³
yd³	cubic yards	0.765	cubic meters	m ³
NOTE: volumes greater than 1000 L shall be shown in m³				
Mass				
oz	ounces	28.35	grams	g
lb	pounds	0.454	kilograms	kg
T	short tons (2000 lb)	0.907	megagrams (or "metric ton")	Mg (or "t")
Temperature (exact degrees)				
°F	Fahrenheit	5 (F-32)/9 or (F-32)/1.8	Celsius	°C
Illumination				
fc	foot-candles	10.76	lux	lx
fl	foot-Lamberts	3.426	candela/m ²	cd/m ²
Force and Pressure or Stress				
lbf	poundforce	4.45	newtons	N
lbf/in²	poundforce per square inch	6.89	kilopascals	kPa

Approximate Conversions from SI Units

Symbol	When You Know	Multiply By	To Find	Symbol
Length				
mm	millimeters	0.039	inches	in
m	meters	3.28	feet	ft
m	meters	1.09	yards	yd
km	kilometers	0.621	miles	mi
Area				
mm ²	square millimeters	0.0016	square inches	in ²
m ²	square meters	10.764	square feet	ft ²
m ²	square meters	1.195	square yards	yd ²
ha	hectares	2.47	acres	ac
km ²	square kilometers	0.386	square miles	mi ²
Volume				
mL	milliliters	0.034	fluid ounces	fl oz
L	liters	0.264	gallons	gal
m ³	cubic meters	35.314	cubic feet	ft ³
m ³	cubic meters	1.307	cubic yards	yd ³
Mass				
g	grams	0.035	ounces	oz
kg	kilograms	2.202	pounds	lb
Mg (or "t")	megagrams (or "metric ton")	1.103	short tons (2000 lb)	T
Temperature (exact degrees)				
°C	Celsius	1.8C+32	Fahrenheit	°F
Illumination				
lx	lux	0.0929	foot-candles	fc
cd/m ²	candela/m ²	0.2919	foot-Lamberts	fl
Force and Pressure or Stress				
N	newtons	02.225	poundforce	lbf
kPa	kilopascals	0.145	poundforce per square inch	lbf/in ²

TECHNICAL REPORT DOCUMENTATION PAGE

1. Report No.	2. Government Accession No.	3. Recipient's Catalog No.	
4. Title and Subtitle <i>Feasibility of atomic and molecular laser induced breakdown spectroscopy (LIBS) to in-situ determination of chlorine in concrete</i>		5. Report Date <i>October 2016</i>	
		6. Performing Organization Code	
7. Author(s) <i>N. Omenetto, E.Ewusi-Annan, T. Guenther, W.B. Jones, B.W. Smith</i>		8. Performing Organization Report No.	
9. Performing Organization Name and Address <i>University of Florida Department of Chemistry Gainesville, FL 32611</i>		10. Work Unit No. (TRAIS)	
		11. Contract or Grant No. <i>00119410 BDV31-977-32</i>	
12. Sponsoring Agency Name and Address <i>Florida Department of Transportation 605 Suwannee Street, MS 30 Tallahassee, FL 32399</i>		13. Type of Report and Period Covered <i>Draft Final Report 11-10-2014 - 10-31-2016</i>	
		14. Sponsoring Agency Code	
15. Supplementary Notes			
16. Abstract			
<p><i>Laser-induced breakdown spectroscopy (LIBS) has been studied as a fast method of detecting chlorine in concrete samples. Both single pulse (SP) and double pulse (DP) experiments have been tested. Several combinations of lasers (Neodymium-Yttrium Aluminum Garnet (Nd:YAG), XeCl, and ArF Excimer lasers with an Intensified Charge Coupled Device (ICCD) detector were used, namely (i) YAG single pulse ablation, (ii) YAG-YAG orthogonal double pulse ablation-excitation, (iii) XeCl-YAG orthogonal double pulse ablation-excitation, and (iv) ArF-YAG double pulse ablation-excitation. An ionic chlorine line at 479.454 nm was then selected, and results optimized in a He atmosphere. Moreover, we have investigated in detail the use of CaCl emission band at 593.5 nm as an alternative detection scheme. The samples (mortar and cement) were provided by the Florida Department of Transportation State Materials Office (Gainesville) and the BAM Institute in Berlin (Germany). Using single-pulse LIBS, the ionic line limit of detection (LOD) was 0.04% Cl, and the molecular CaCl band LOD was 0.05%. Both results were obtained in a He environment. Contrary to expectations and to literature results, our double pulse experiments did not improve the detection limit.</i></p> <p><i>The results obtained in this report are discussed in terms of the following criteria: (i) achievement of the original goals of the project achieved; (ii) the analytical validity of the proposed approach and the benefits resulting from the implementation of the developed technique in a different laboratory; and (iii) the importance of "in situ" detection of Cl in concrete and of a mobile LIBS system for stand-off operation.</i></p>			
17. Key Word <i>laser-induced breakdown spectroscopy (LIBS), chlorine detection in concrete, molecular CaCl emission, single-pulse and double-pulse LIBS, limit of detection (LOD)</i>		18. Distribution Statement No restrictions	
19. Security Classif. (of this report) Unclassified	20. Security Classif. (of this page) Unclassified	21. No. of Pages 52	22. Price

ACKNOWLEDGEMENTS

The authors would like to acknowledge the many discussions and interest shown by the officers of the Florida Department of Transportation State Materials Office (Gainesville) during the course of this project. In particular, we would like to thank Mr. Steven Schein and Mr. Paul Vinik for the initial contact and ensuing discussion, which originated the present work.

We would also like to acknowledge the initial interest and help of Mr. Paul Gleason of the Florida Department of Transportation State Materials Office (Gainesville) for the information provided on the basic preparative chemistry and characterization of the concrete samples and for preparing for us several samples of concrete at known concentrations of chlorine, which were used for calibration.

Special thanks are finally due to Dr. Igor Gornushkin, Dr. Gerd Wilsch, and Dr. Ulrich Panne of the Federal Institute for Materials Research and Testing (BAM) in Berlin (Germany) for sharing scientific information pertinent to chlorine detection and in particular for providing a series of standard reference samples containing chlorine in the low concentration range (blank-2.2%).

EXECUTIVE SUMMARY

Laser-induced breakdown spectroscopy (LIBS) has been studied as a fast method of detecting chlorine in concrete samples. Both single pulse (SP) and double pulse (DP) experiments have been tested. Several combinations of lasers (Neodymium-Yttrium Aluminum Garnet (Nd:YAG), XeCl, and ArF Excimer lasers with an Intensified Charge Coupled Device (ICCD) detector were used, namely (i) YAG single pulse ablation, (ii) YAG-YAG orthogonal double pulse ablation-excitation, (iii) XeCl-YAG orthogonal double pulse ablation-excitation, and (iv) ArF-YAG double pulse ablation-excitation. The most common chlorine neutral atom line reported in the literature at 837.6 nm was not analytically useful in our case, due to the low spectral response of our ICCD at that wavelength. An ionic chlorine line at 479.454 nm was then selected, and results optimized in a He atmosphere. Moreover, we have investigated in detail the use of CaCl emission band at 593.5 nm as an alternative detection scheme to the use of atomic chlorine emission in the near IR (837.6 nm) or ionic emission of the Cl^+ triplet around 480 nm. The use of CaCl molecular emission to detect Cl with LIBS has been reported before, although with no detailed analytical discussion.

Samples were provided by the Florida Department of Transportation State Materials Office (Gainesville) and the Federal Institute for Materials Research and Testing in Berlin (Germany). Using single-pulse LIBS and the standard DIN 32645 protocol for calculating the limit of detection (LOD) from the calibration curve, slope, and intercept of the data, the ionic line LOD was 0.04% Cl, and the molecular CaCl band LOD was 0.05%. Both results were obtained in a He environment. Contrary to expectations and to literature results, our double pulse experiments did not improve the detection limit to an extent significant enough to justify the added instrumental complexity. The result of the combination ArF-YAG was not successful, due mainly to the low energy of the ArF laser. This laser, however, will be useful for investigating possible photochemical effects on the molecular emission kinetics of CaCl. Such study was considered out of the scope of the present work.

The results obtained in this report are discussed in terms of the following criteria: (i) how close were the original goals of the project obtained; (ii) the analytical validity of the proposed approach and the benefits resulting from the implementation of the developed technique in different analytical laboratories; and (iii) the relevance of “in situ” detection of Cl in concrete and of constructing a mobile LIBS system for stand-off operation.

TABLE OF CONTENTS

DISCLAIMER PAGE.....	ii
METRIC CONVERSION CHART.....	iii
TECHNICAL REPORT DOCUMENTATION PAGE.....	v
ACKNOWLEDGEMENTS.....	vi
EXECUTIVE SUMMARY.....	vii
LIST OF FIGURES.....	ix
LIST OF TABLES.....	xi
LIST OF ABBREVIATIONS AND ACRONYMS.....	xii
INTRODUCTION.....	1
CHAPTER 1. SINGLE-PULSE LIBS (SP-LIBS) DETECTION OF CHLORINE IN CONCRETE.....	3
CHAPTER 2. DOUBLE-PULSE LIBS DETECTION OF CHLORINE IN CONCRETE.....	14
CHAPTER 3. SINGLE-PULSE LIBS DETECTION OF CHLORINE IN CONCRETE USING CaCl EMISSION.....	23
CHAPTER 4. OVERALL CONCLUSIONS AND ANALYTICAL CONSIDERATIONS.....	33
REFERENCES.....	36

LIST OF FIGURES

Figure 1-1. Basic single-pulse LIBS experimental setup.....	3
Figure 1-2. Simplified energy level diagram pertinent to the chlorine transitions investigated in this report. <i>Left</i> : neutral atom; <i>Right</i> : atomic ion.....	5
Figure 1-3. Experimental result obtained with pellets containing 1% NaCl in Cu matrix. <i>Left</i> : spectral line: 837.595 nm; <i>Right</i> : spectral line: 725.663 nm.....	5
Figure 1-4. Experimental images obtained in the spectral region showing the triplet of ionic chlorine lines reported in Fig. 1-2. <i>Left</i> : Ambient air; <i>Right</i> : He.....	6
Figure 1-5. Spectral width of a Ca II ion line in three different environments, i.e., He, air, and Ar.....	6
Figure 1-6. <i>Left</i> : Craters ablated on a concrete sample. <i>Right</i> : profile measured with a white light interferometer (Bruker) at the Nanoscale Research Facility, UF.....	7
Figure 1-7. Experimentally observed temporal behavior of the chlorine and background signals.....	7
Figure 1-8. Chlorine signature at 479.454 nm for 10 independent FDOT concrete samples containing 0.5% NaCl (0.3% Cl) (<i>top</i>) and 1% NaCl (0.6% Cl) (<i>bottom</i>).....	8
Figure 1-9. Shot-to-shot variability in the experimental data obtained with NaCl concentrations of 2.5% (<i>left</i>) and 5% (<i>right</i>).....	9
Figure 1-10. <i>Left</i> : Spectral intensity of the 479.454 nm chlorine line (average of 570 laser shots on individual DOT sample in the NaCl concentration range indicated in the insert). <i>Right</i> : Standard deviation spectral behavior.....	9
Figure 1-11. <i>Left</i> : Experimental spectrum obtained under optimized measurement conditions for a <i>single</i> FDOT sample containing 0.3% Cl. <i>Right</i> : Calibration curve in the range “blank”-1% Cl.....	10
Figure 2-1. Orthogonal double-pulse LIBS operating principle. <i>Adapted</i> from [3].....	15
Figure 2-2. Orthogonal double-pulse LIBS experimental setup. o.a.=optical axis.....	15
Figure 2-3. <i>Left</i> : Experimental enhancement effect observed for an inter-pulse delay (IPD) of 1 μ s. <i>Right</i> : Same experiment as in the left figure, except for the IPD, which has been set at 5 μ s.	16
Figure 2-4. Temporal behavior of the enhancement effect due to the re-heating pulse.....	16

Figure 2-5. <i>Left</i> : Net peak signal to background ratio (P/B) and enhancement factor as a function of IPD. <i>Right</i> : Temporal behavior of the S/N ratio as a function of IPD.....	17
Figure 2-6. Temporal behavior of the RSD of three analytical figures of merit, i.e., P, B, and (P+B), as a function of IPD. The enhancement factor is shown for comparison.....	17
Figure 2-7. <i>Left</i> : Temporal behavior of the chlorine triplet observed in the pre-spark mode using two Nd-YAG lasers at 1064 nm. <i>Right</i> : Enhancement versus delay.....	18
Figure 2-8. Enhancement effect observed in the re-heating mode using the combination XeCl/Nd-YAG lasers.	18
Figure 2-9. Same as figure 2-8, except that here the spectrum obtained with the XeCl laser alone is shown (black trace) and the IPD has been set to 1.0 μ s.	19
Figure 2-10. Comparison between single-pulse and double-pulse spectra obtained in the pre-spark mode with YAG/YAG combination.	19
Figure 3-1. Temporal evolution of the CaCl band at 593.5 nm taken with the 1,200 gr/mm grating. <i>Top (left and right)</i> : air; <i>Bottom (left and right)</i> : He. Sample: FDOT 3% Cl.....	24
Figure 3-2. Temporal evolution of the signal-to-background ratio (S/B) (<i>left</i>) and net signals (<i>right</i>) relative to molecular and atomic emission of CaCl, Na, and Ca.	25
Figure 3-3. Temporal evolution of the CaCl band emission in He. Sample: BAM 2.26% Cl....	26
Figure 3-4. Analytical behavior of the signal-to-background ratio as a function of the gate delay (<i>left</i>) and gate integration time (<i>right</i>).	26
Figure 3-5. Temporal behavior of several species relevant to the kinetics of formation of CaCl in the plasma (different delays indicated in the x-axis).....	27
Figure 3-6. Analytical signals obtained at different chlorine concentration concentrations in the low percent range, as indicated in the box.....	28
Figure 3-7. Same as Fig. 3-6, except that the experiment was performed in He.....	28
Figure 3-8. Analytical improvement resulting from normalizing (pixel by pixel) the spectra for various sample concentrations to the lowest concentration spectrum (assumed equivalent to a <i>blank</i> spectrum).	29
Figure 3-9. Calibration curve obtained in the ambient air by plotting the S/B ratio as a function of Cl concentration in the range 0.08-1% Cl.	30
Figure 3-10. Calibration curve obtained in the He environment by plotting the S/B ratio as a function of Cl concentration in the range 0.08-1% Cl.....	30

LIST OF TABLES

Table 1-1: Conversion factors, pertinent to this report, expressing the numerical relations between the different units found in the literature when expressing chlorine concentration in concrete. The density of the Portland cement and the “rejection” concentration reported here have been provided by FDOT	11
Table 1-2: Single-pulse laser-induced breakdown spectroscopy detection of chlorine in various samples as reported in the literature cited in this report: a survey	12
Table 4-1: Review of total chloride threshold values (taken from ref. 56).....	34

LIST OF ABBREVIATIONS AND ACRONYMS

BAM: Bundesanstalt für Materialforschung und -prüfung (Federal Institute for Materials Research and Testing)

CCD: Charge Coupled Device

CHEMCAM: Chemistry & Camera (stand-off LIBS analysis of rocks and soil on Mars)

DP-LIBS: Double-Pulse Laser-induced Breakdown Spectroscopy

EMSLIBS: European Mediterranean -LIBS

FDOT: Florida Department of Transportation

FWHM: Full Width at Half Maximum

ICCD: Intensified Charge Coupled Device

IPD: Inter-pulse Delay time

LIBS: Laser-induced Breakdown Spectroscopy

LOD: Limit of Detection

LOQ: Limit of Quantitation

LTE: Local Thermodynamic Equilibrium

OMA: Optical Multichannel Analyzer

P/B: Peak signal to Background Ratio

RSD: Relative Standard Deviation

SD: Standard Deviation

S/N: Signal to Noise Ratio

SP-LIBS: Single-Pulse Laser-induced Breakdown Spectroscopy

Nd-YAG: Neodymium-Yttrium Aluminum Garnet laser

TEA-CO₂: Transversely Excited Atmospheric-Carbon Dioxide laser

INTRODUCTION

The present report describes and discusses three experimental approaches tested in the laboratory to assess the sensitivity and specificity for detection and quantitative determination of chlorine in concrete samples by the technique of laser-induced breakdown spectroscopy (LIBS). The general relevance of this topic is obvious for the structural safety of concrete construction. Also, it is understandable that LIBS has been used for this type of analysis, due to its unique advantages of marginal sample preparation and stand-off detection capabilities [1-3]. Of special significance is the fact that LIBS instrumentation can be configured to be easily portable and implemented in the field. On the other hand, detecting chlorine by emission spectroscopy is a very challenging task *per se*, due to the fact that its strongest resonance lines are in the vacuum UV (~138 nm), and the near IR transitions (752, 837 nm) are less intense, more prone to spectral interferences, requiring optimized detector efficiency.

In the literature, both single-pulse (SP-LIBS) and double-pulse (DP-LIBS) approaches have been described. In SP work, a limit of detection of 500 ppm has been reported [4]. Double-pulse operation requires two lasers arranged in a collinear or orthogonal configuration [3] and can provide significant signal enhancement with a corresponding improvement of the limit of detection. Using DP-LIBS, limits of detection in the range 10-100 ppm have been reported [4-6]. Translating these numbers in the commonly used way of expressing concentration in the field of cement analysis (see Table 2), 10-100 ppm corresponds to 0.064-0.64 lb/cu yd (1 lb/cu yd = 156 ppm, assuming a density of 3,800 lb/cu yd), meaning that a realistic limit of quantitation should range from 0.01% to 0.1% Cl by weight. If a “corrosion limit” (resulting in rejection of the material) is set at 0.8 lb/cu yd (125 ppm), that should indeed be considered closer to the limit of quantitation rather than to a limit of detection.

It is also well known that chloride compounds emit molecular bands in the UV-VIS region of the spectrum. Vibro-rotational band structure of molecules such as CaCl, SrCl, and MgCl are well characterized in the literature (see Chapter 3). Due to the high temperature of the plasma, molecular LIBS has not been widely investigated until recently [3]. The only previous attempt to detect chlorine in gases by molecular emission was reported in 1996 using a combination of LIBS on a copper target and molecular emission of CuCl in a flame [7]. In view of the high concentration of Ca in cement, it seems logical to investigate the analytical potential of using CaCl band emission to quantify chlorine in this material.

Since the beginning of 1970, the laser spectroscopy laboratory of the Department of Chemistry at the University of Florida has been involved in fundamental and applied laser spectroscopy work, including absorption and fluorescence spectroscopy. Relevant to this report, in the last 20 years, the laboratory has developed LIBS methodology and instrumentation (including portable systems) and produced a large number of publications on this topic. Recently, in response to a request of the Florida Department of Transportation (FDOT) in Gainesville, an *ad hoc* system was assembled allowing single-pulse and double-pulse LIBS operation to study the analytical potential of these methodologies to detect and quantify chlorine in concrete samples. The present report aims first at describing the results obtained using three different approaches and, second, at discussing these results in light of the following criteria: (i) how close were the original goals of the project obtained; (ii) the analytical validity of the

proposed approach and the benefits resulting from the implementation of the developed technique in different analytical laboratories; and (iii) the relevance of “in situ” detection of Cl in concrete and of constructing a mobile LIBS system for stand-off operation.

CHAPTER 1. SINGLE-PULSE LIBS (SP-LIBS) DETECTION OF CHLORINE IN CONCRETE

1.1: Literature survey

40 references are provided. Most of these refer to specific work on chlorine detection by LIBS. A recent LIBS book [1] and two general reviews [2,3] are listed. Apart from a few references to chlorine detection by other techniques, e.g., ICP emission and Mass Spectrometry, X-ray Fluorescence [8-11], one reference to a line profile [29], and 11 references to the definition and practical use of limits of detection, calibration curves and homogeneity problems [30-40], all other references deal with Cl detection by LIBS.

Table 1 collects several conversion factors that are useful to convert the Cl concentration in the various units more commonly reported in the literature. Table 2 collects the most pertinent work done in other laboratories, the type of samples analyzed and the LOD obtained with Single-Pulse LIBS. For the sake of completeness, the values obtained in our work are also reported.

1.2: Setup SP-LIBS instrumentation

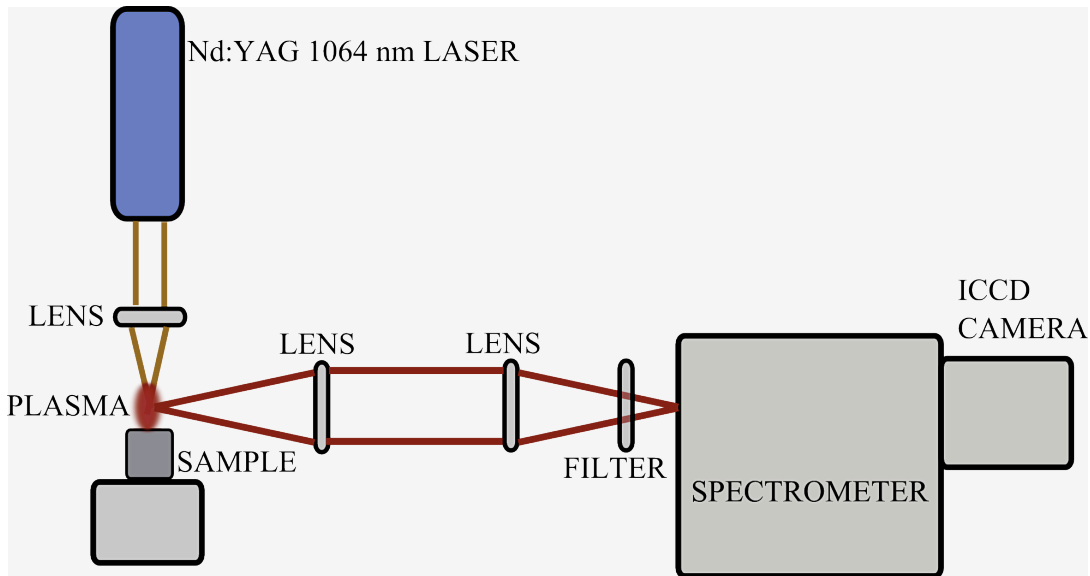


Figure 1-1. Basic schematic of the single-pulse LIBS experimental setup used in this report.

The set-up used is shown in Figure 1-1. The ablation laser is a Nd:YAG pulsed laser (Brilliant, Quantel Inc., USA) with the following characteristics: operating wavelength: 1064 nm; variable pulse energy up to 320 mJ/pulse (see below); pulse width: 6 ns FWHM; maximum repetition frequency: 10 Hz. The laser is focused on the sample using a 5.0 cm focal length biconvex lens. The sample can be enclosed in a cell filled with He and mounted on xyz translational stage for precise location adjustment. The resulting plasma is collimated using a quartz plano-convex lens placed at its focal distance from the plasma and then focused on the entrance slit of the monochromator using another plano-convex lens. Neutral density and interference filters are used to ensure linear operation of the detector and to avoid second order

overlapping. Matching of the lens-monochromator F -numbers can be optimized by an adjustable iris placed between the focusing lens and the entrance slit of the spectrometer. The use of an optical fiber to collect the plasma radiation did not improve the collection efficiency.

The 0.5 m spectrometer (SpectraPro 500i, Acton, USA, F/6.5) is equipped with three gratings (1,200, 2,400, and 3,600 grooves/mm), providing a reciprocal linear dispersion of 1.57, 0.72, and 0.41 nm/mm, respectively. The detector is an intensified charge coupled device (ICCD)(PI-MAX2, Princeton Instruments, USA) with an array of 1024 x 1024 pixels, each pixel having a size of 13 x 13 μm . Each pixel has a well capacity of 65,000 counts. This represents the maximum number of charges a pixel can accommodate before a spill over into adjacent wells.

The timing between the laser triggering and the detection of plasma emission by the ICCD is accomplished with a delay generator (DG-535, Stanford Research, USA). The laser energy is changed by adjusting the time delay between the flash lamp and the Q-switch triggers, without taking into account possible variations in the pulse duration or its temporal profile. This practice, which is not recommended for accurate diagnostic measurements of the physical plasma parameters (e.g., excitation temperature and electron number densities) and for checking the existence of Local Thermodynamic Equilibrium (LTE) conditions, is nevertheless convenient and easy to implement. The internal delay generator of the ICCD is used for time-resolved acquisitions. The overall experimental settings are controlled using Winspec32 software (Version 2.5, Princeton Instruments, USA).

1.3. Choice of the analytical line

A schematic diagram of the energy levels involved in the transitions, together with their spectroscopic nomenclature and the level energies are shown in Figure 1-2. The wavelengths are indicated in nm and the numbers associated with the transitions are the known values of the spontaneous transition probabilities (Hz). The spectra shown in the inserts have been taken with the instrumentation described in Fig. 1-1.

The energy levels are indicated in eV . The diagram explains the difficulty alluded to earlier of detecting this element, since the energy difference between the ground state and the excited state lies in the vacuum ultraviolet (134.724 nm). This explains why this line has not been widely used for the detection of chlorine. The lines indicated in red in the left part of Figure 1-2 are in the near infrared and are normally plagued with potential spectral interferences from ambient lines due to air constituents (oxygen and nitrogen).

The right side of fig. 1-2 shows the pertinent energy levels of the chlorine ion and therefore starts with the ground state energy corresponding to the first ionization limit of the neutral atom. In this case, the three transitions in the blue region of the spectrum have been chosen in our work.

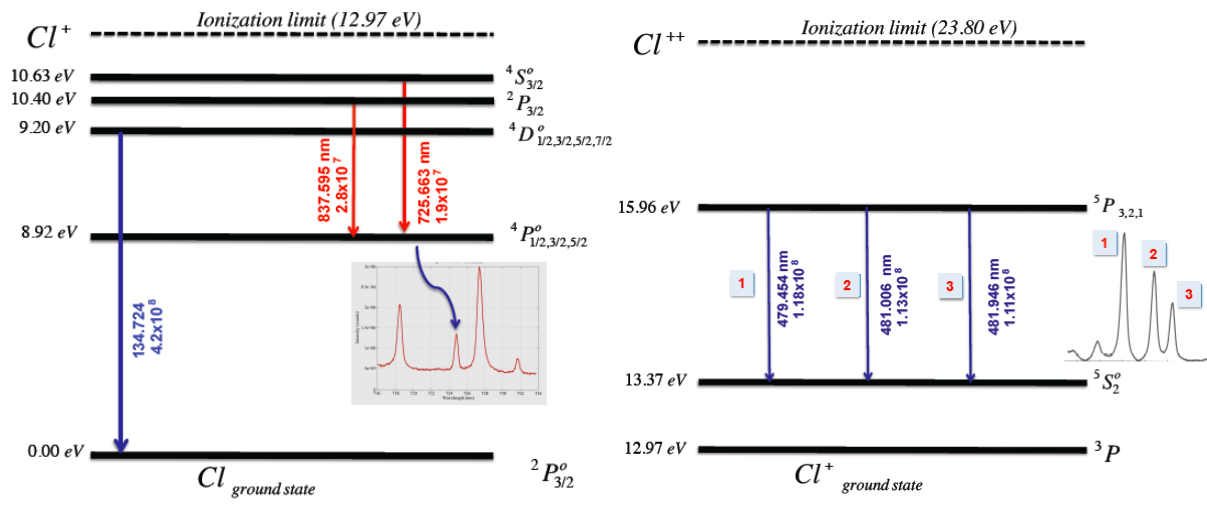


Figure 1-2. Simplified energy level diagram pertinent to the chlorine transitions investigated in this report. *Left*: neutral atom; *Right*: atomic ion.

Our ICCD camera is not sensitive in the near-infrared (see Figure 1-3). The comparison between the left and right figures shows the poor sensitivity of our set-up in the near infrared, where the Cl line at 837.595 nm is barely distinguishable from the background. Note that the shape of the spectral background varies with the spectral region investigated.

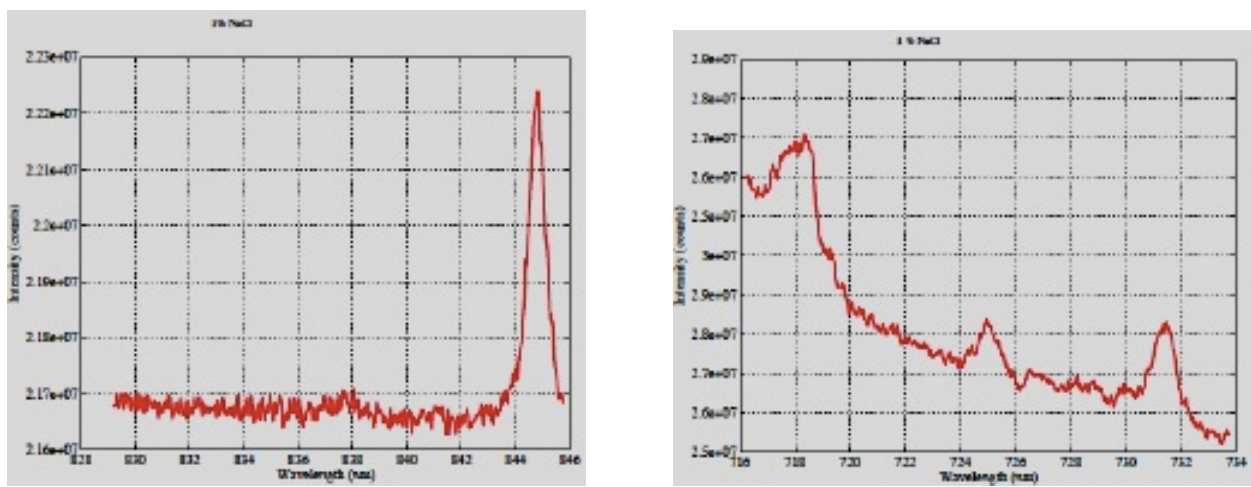


Figure 1-3. Experimental result obtained with pellets containing 1% NaCl in Cu matrix. *Left*: spectral line: 837.595 nm; *Right*: spectral line: 725.663 nm.

Most references on chlorine detection reported here make use of the atomic line at 837.595 nm. We have been able to use the line at 725.663 nm with some success. Nevertheless, note that the spectrum shown at the right side of Fig. 1-3 was obtained in a copper matrix, and cannot be assumed to be the same when the concrete matrix is ablated in the same conditions. Our best results have been obtained with the atomic ion line at 479.454 nm. Note that, apart from earlier measurements carried out at BAM, this line has seldom been utilized for chlorine detection in concrete. This chapter will therefore focus on the results obtained by using this line.

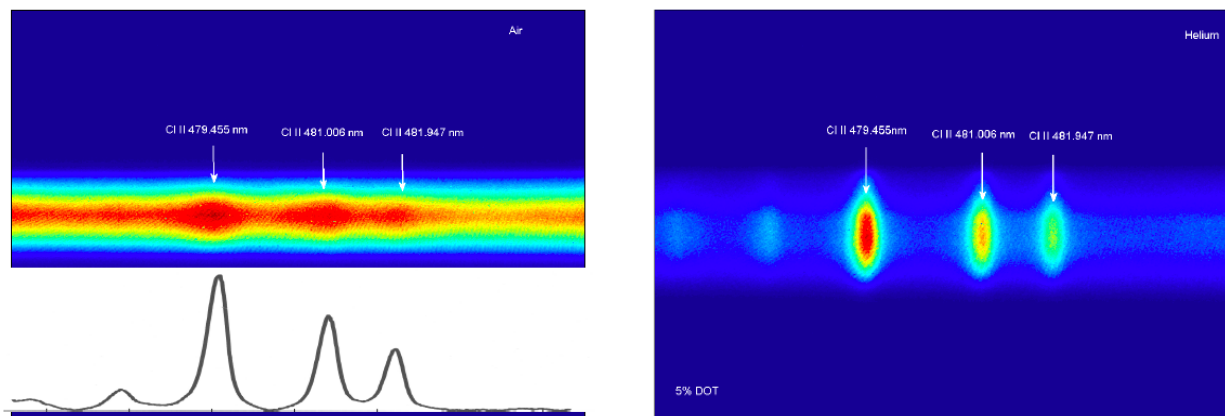


Figure 1-4. Experimental images obtained in the spectral region showing the triplet of ionic chlorine lines reported in Figure 1-2. *Left*: Ambient air; *Right*: He.

In agreement with several literature publications, we have used a He flow around the sample during measurements. As shown in Figure 1-4, the intensity of the triplet lines is still significant while the background decreases considerably. This is due to the lower number density of electrons (n_e) in the plasma created, as seen in figure 1-5 by the smaller line width of a Ca II transition in three environments (He, air, and Ar), with the consequence that the laser pulse is less attenuated by the plasma, leading to a more efficient interaction with the sample and more mass ablated. As reported in the literature [see, e.g., 19] a plausible explanation for the beneficial effect of He is that the lower electron number density results in a lower background emission and a better interaction of the target with the ablating laser pulse.

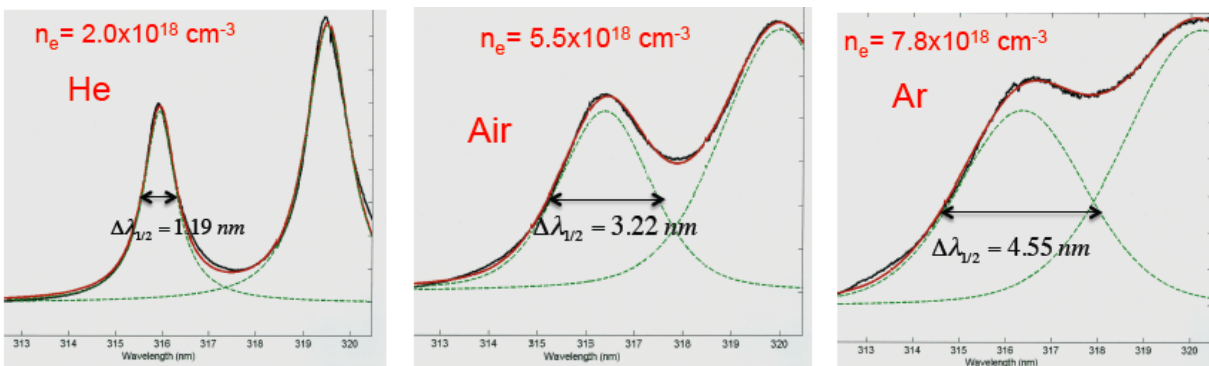


Figure 1-5. Spectral width of a Ca II ion line in three different environments, i.e., He, air, and Ar.

It was found that the mass ablated increases with the laser energy. This was experimentally demonstrated by measuring the crater volume formed at different sample locations (see figure 1-6). From the calculated volume and the density of sample, the mass ablated by the laser can be estimated. The crater volume and the corresponding signal intensity increase with increasing laser pulse energy. From the density of the concrete, one calculates that several micrograms per pulse can be released in the plasma. Note, however, that not all the ablated mass contributes to the analytical signal.

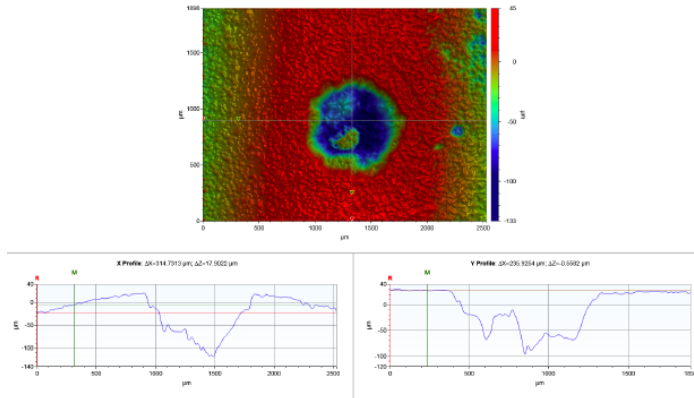


Figure 1-6. *Left*: Craters ablated on a concrete sample. *Right*: profile measured with a white light interferometer (CountourGT, Bruker) at the Nanoscale Research Facility, University of Florida.

The problem in the choice of an ionic line is that the ion formation occurs at the very beginning of plasma formation and then the ion population decays due to recombination effects and plasma cooling. This can be seen in Figure 1-7. In the figure, the X-axis shows the time delay used before the opening of the measuring gate. The width of the gate is fixed at 200 ns. The figure shows clearly that the signal decays rapidly to the baseline level, and that after approximately $1 \mu\text{s}$, the chlorine signal becomes undetectable. This means that the use of integration times longer than $1 \mu\text{s}$ will not increase the signal level and on the contrary will decrease the signal-to-background ratio.

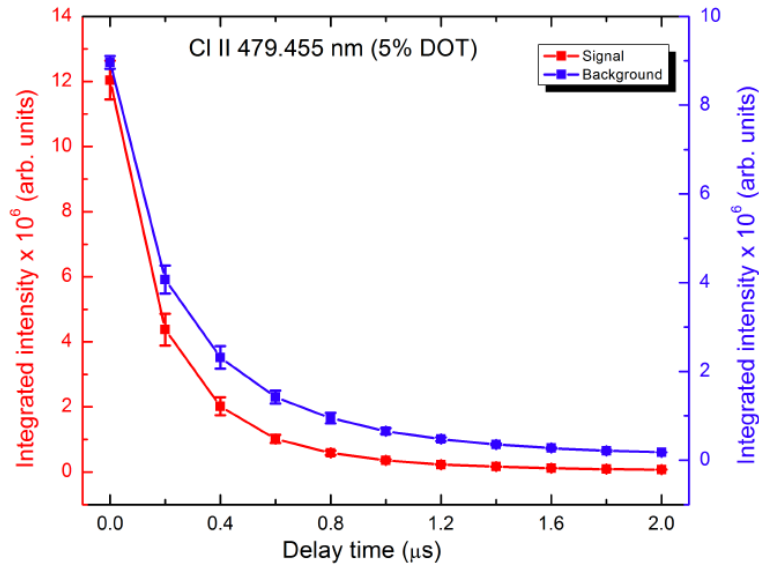


Figure 1-7. Experimentally observed temporal behavior of the chlorine and background signals.

1.4. Evaluation of the limit of detection. Data analysis

One of the problems encountered with this type of analysis is the heterogeneity of the sample. We have worked with standard concentrations prepared at the FDOT facility in Gainesville (Paul Gleason).

However, a much better estimate of the sample-to-sample variability was obtained using the following procedure: 10 independent FDOT samples containing the same nominal concentration of NaCl were sequentially ablated and the chlorine signal measured. Three different locations on each sample were randomly chosen. For each location, 20 laser shots were accumulated. Therefore, each sample provided 60 spectra and a total of 600 spectra were stored at the end of the measurement cycle. Due to an artifact of the acquisition routine, the first spectrum was always discarded, leaving a total of 57 spectra (instead of 60) per sample. The total number of single laser shot spectra subsequently analyzed was therefore 570.

An example of the results obtained is given in Figures 1-8 to 1-10. Note that this procedure allows not only to calculate the average background, gross signal (net Cl signal plus background) and net signal (gross signal minus background), but it also allows calculating the standard deviation (SD) and relative standard deviation (RSD) of each wavelength of the spectral range investigated (see figure 1-10).

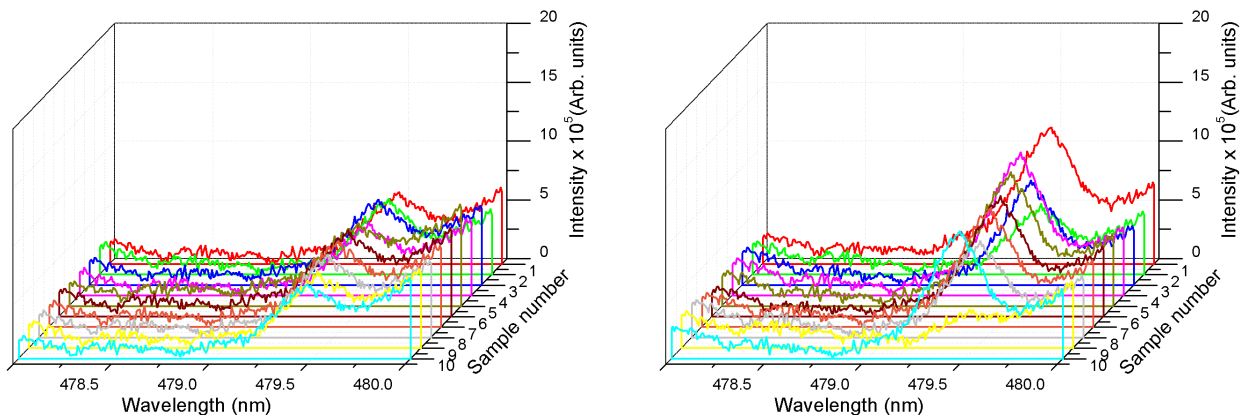


Fig. 1-8. Chlorine signature at 479.454 nm for 10 independent FDOT concrete samples containing 0.5% NaCl (0.3% Cl) (*left*) and 1% NaCl (0.6% Cl) (*right*).

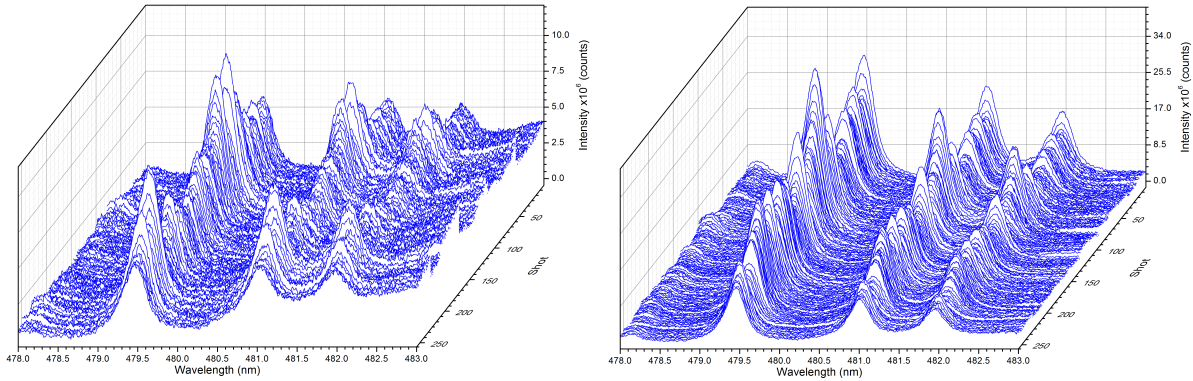


Figure 1-9. 3D plots showing the shot-to-shot variability in the experimental data obtained with NaCl concentrations of 2.5% (1.5% Cl) (*left*) and 5% (3% Cl)(*right*).

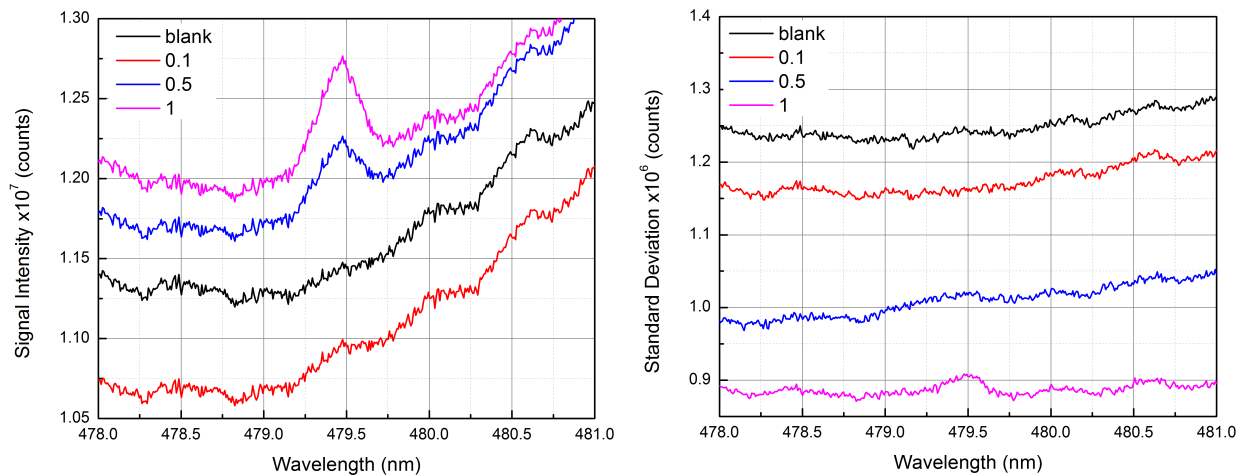


Figure 1-10. *Left*: Spectral intensity of the 479.454 nm chlorine line (average of 570 laser shots on individual FDOT sample in the NaCl concentration range indicated in the insert). *Right*: Standard deviation spectral behavior.

Three observations were made:

(i) The background signal varies from sample to sample. Because the chlorine signal has to be measured at early delays (close to zero) in the plasma temporal evolution, background emission and its associated fluctuations dominate the measurements and is the main reason for the observed noise; (ii) the best LOD has been obtained by optimizing the acquisition parameters (gate integration, slit width, number of accumulations) and collecting the signal from different randomly selected locations in a single FDOT sample containing 0.5% NaCl. Based on the S/N ratio of 3, the LOD was calculated to be 0.02% Cl (see Figure 1-11, left).

(ii) Note that the blank, prepared in the same way as the “standard” concrete samples *without* the addition of NaCl, can be considered as the “background equivalent concentration” of chlorine in the DOT concrete samples provided. Note that the background variability is real, i.e., the curves in the plots have not been vertically displaced for clarity. The relevance of plotting the

spectral behavior of the standard deviation has been discussed by Hahn and Omenetto [3]: the presence or absence of peaks at the position of the analytical lines indicates the type of noise limiting the measurement.

(iii) The calibration curves obtained from Figure 1-10 in the low concentration range of Cl (blank to 0.6%) are shown in figure 1-11. The operating conditions were the following: Laser energy: 300 mJ/pulse; delay time: minimum (nominally zero); integration time: 1 μ s; slit width: 200 μ m; 120 shots accumulation; manual sample displacement during measurement; background subtracted.

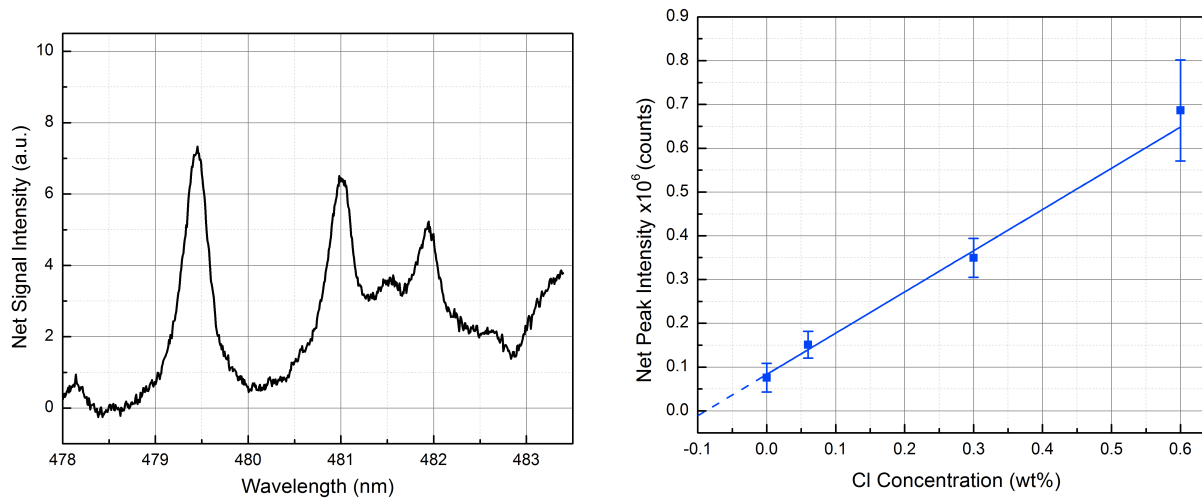


Figure 1-11. *Left*: Experimental spectrum obtained under optimized measurement conditions for a single FDOT sample containing 0.5% NaCl (0.3% Cl). *Right*: Calibration curve in the range blank-1% Cl.

The signal-to-background noise ratio of 3 calculated for the 479.454 nm gives a detection limit of 0.04 % NaCl (0.02% Cl). The error bars are the standard deviation of the net signal measured at the peak of the Cl signal. The application of the DIN 32645 protocol for calculating the LOD from the calibration curve, slope, and intercept of the data of the right figure results in an LOD of 0.04% Cl

1.5. Conclusions

(i) SP-LIBS using an ionic line of chlorine gave the best results for our instrumental set-up. It is worth noting again that, to our knowledge, this line has not been studied by other researchers (see Table 1-2). It is fair to say that the background associated with its use will always dominate the measurement, since the persistence of ion emission in the plasma is short. Despite that, our detection limit compares favorably with those reported in the literature, being approximately a factor of 2 higher than the best limit reported so far, i.e., 0.008% Cl.

(ii) The limiting Cl value for rejection (*corrosion limit*) communicated by FDOT is \sim 200 ppm (\sim 0.02%). Such value is practically the same as our detection limit. It is therefore fair to say that such a low *corrosion limit* cannot be *quantified* by our system, or even by all systems

reported in Table 1-2, with the exception of that of Sugiyama et al.[5], who quoted 80 ppm as their detection limit. It is also worth stressing, however, that Angst et al. [26] pointed out that there are different definitions of *critical content* or *critical threshold* value of chlorine in reinforced concrete. As an example, Weritz et al. [12] have reported *critical* chlorine contents relative to the cement mass of concrete to be in the range 0.2-0.4%. Taking into account that the *limit of quantification* (LOQ) is normally calculated for a S/N=10 (rather than S/N=3), our results indicate that these critical values can indeed be quantified.

Table 1-1: Conversion factors, pertinent to this report, expressing the numerical relations between the different units found in the literature when expressing chlorine concentration in concrete. The density of the Portland cement and the “rejection” concentration reported here have been provided by FDOT.

- $1 \text{ lb} = 0.4536 \text{ kg}$
- $1 \text{ cu yd} = 0.7646 \text{ m}^3$
- $1 \text{ yd} = 0.9144 \text{ m}$
- $1 \frac{\text{lb}}{\text{cu yd}} = 0.5933 \frac{\text{kg}}{\text{m}^3}$ • $1\% \text{ (by weight)} = 10,000 \text{ ppm}$
- $\text{Density of Portland cement} = 3,800 \frac{\text{lb}}{\text{cu yd}} = 2,254.5 \frac{\text{kg}}{\text{m}^3}$
- $1 \frac{\text{kg}}{\text{m}^3} (\text{Cl}) = 443 \frac{\text{mg}}{\text{kg}} (\text{Cl}) = 443 \text{ ppm} (\text{Cl}) \text{ in cement}$
- $1 \frac{\text{lb}}{\text{cu yd}} (\text{Cl}) = 262.8 \text{ ppm} (\text{Cl}) \text{ in cement}$
- $\text{Chlorine concentration for rejection} : 0.08 - 0.8 \frac{\text{lb}}{\text{cu yd}} = 21.04 - 210.4 \text{ ppm}$

Table 1-2. Single-pulse Laser induced Breakdown Spectroscopy detection of chlorine in various samples as reported in the literature cited in this report: A survey (*)

Laser Type	Characteristics	Spectrometer Spectral resolution (nm)	Detector	Cl line used (nm)	Sample and operating conditions	LOD (Cl)			Literature-first author -[ref.no]
	λ (nm), Δt_p (s), E_p (mJ/pulse), f (Hz)					(mass %)	lbs/(cu yd)	kg/m ³	
Nd:YAG	1064; 5 ns; 100 mJ/pulse; 1 Hz	Grating spectrometer; 0.05	ICCD	Cl I 837.595	Solid organic Compound; Air/He	0.00088 (mole fraction)			Tran [18]
TEA-CO ₂	10.6 μ m; 200 ns; 3 J/pulse; 5 Hz	Grating spectrometer; 0.18	OMA (CCD)	Cl II 479.454	Solid organic Compound; Air/He	-			Idris [28]
Nd:YAG	355 nm; 10-26 mJ/pulse; 5 Hz	Grating spectrometer	ICCD	Cl I 837.595	Pharmaceuticals; He / Low Pressure	0.375	14.3	8.47	Asimellis [19]
KrF	248 nm; 12 ns; 5 mJ/pulse; 15 Hz	Purged spectrometer	ICCD	Cl I 134.724	Solid organic compounds	0.054 Cl/C (atomic ratio in the sample)			Kaski [27]
Nd:YAG	1064; 8.5 ns; 450-480 mJ/pulse; 50 Hz	Paschen-Runge Vacuum Spectrometer	Multi-channel Integrator	Cl I 134.724 Cl I 837.595	Cement – Concrete drill cores	0.1 0.2	4 8	2 5	Gehlen [22]
Nd:YAG	1064; 10 ns; 400 mJ/pulse; 20 Hz	Grating spectrometer	OMA (CCD)	Cl I 837.595	Concrete Air/He	0.15	5.7	3.4	Wilsch [23]
Nd:YAG	1064; 10 ns; 400 mJ/pulse; 10 Hz	Grating spectrometer	CCD	Cl I 837.595	Concrete Air/He	0.15	5.7	3.4	Weritz [12]
Nd:YAG	1064; 10 ns; 300 mJ/pulse	Grating spectrometer; 0.08	Compare CCD's	Cl I 837.595	Hydrated cement-mortar(He)	0.5	20	10	Weritz [13]
Nd:YAG	1064 nm; 9 ns; 120 mJ/pulse; 10 Hz	Grating spectrometer (4 channels)	Gated detection	Cl I 594.858	Reinforced concrete (Air)	0.2	8	5	Gondal [17]
Nd:YAG	532 nm; 200 mJ/pulse; 10 Hz	Grating spectrometer	ICCD	Cl I 837.595 nm	Concrete Air/He	0.008 (**)	0.3	0.2	Sugiyama [5]
Nd:YAG	1064 nm; 7 ns; 320 mJ/pulse; 1 Hz	Grating spectrometer; 0.035 (50 μ m slit)	ICCD	Cl II 479.454 nm	DOT Cement Mortar Mixes (#)	0.1 (Fig. 1-10) 0.02 (Fig. 1-11) 0.04 (Fig. 1-11)	4 0.8 2	2 0.5 1	This Report

Table 1-2 (*continued*). Single-pulse Laser induced Breakdown Spectroscopy detection of chlorine in various samples as reported in the literature cited in this report: A survey (*)

(*)

The laser characteristics reported are the wavelength of operation (λ), the pulse width (Δt_p), the energy per pulse (E_p), and the repetition rate (f). (Cl I means that the line used is an atomic neutral atom line and Cl II is an atomic ion line. CCD: Charge Coupled Device; ICCD: Intensified Charge Coupled Device. Except in the two cases indicated, where mole fractions are given, the LOD's are reported in mass% of Cl, lbs/(cu yd), and Kg/m³.

(**)

This limit was calculated using a S/N ratio of 2.

(#)

Cement + Fine aggregate + Water + NaCl (Paul Gleason, FDOT, personal communication).

CHAPTER 2. DOUBLE-PULSE LIBS DETECTION OF CHLORINE IN CONCRETE

2.1: Literature survey

The pertinent references specifically dealing with double-pulse experiments are listed in the bibliography at the end of this report. Five studies are listed: one [4] uses an electrical discharge instead of another laser to enhance the signal, three [6,15,22] use two lasers in the *collinear configuration* (both lasers interacting directly with the sample), and one paper describes the use of two lasers in the *orthogonal* configuration [5]. This last work is the only one close to the work done in our laboratory in terms of characterization of the enhancement and associated parameters. However, all works make use of neutral atomic lines of Cl (mostly the 837.59 nm line) instead of the ionic transition at 479.45 nm chosen in our experiment. As a result, the existing double-pulse literature on chlorine in concrete is of limited use.

2.2: Setup of DP-LIBS instrumentation

The basic operating principle of double-pulse LIBS and its laboratory implementation are illustrated in Figure 2-1 and 2-2. The excimer laser (ArF or XeCl) ablates the sample, while the Nd-YAG laser crosses the excimer laser *orthogonally* in front of the sample (see figure on the right).

As can be seen from the figures, this scheme is called the “orthogonal” scheme, since only one laser (the ablation laser) interacts directly with the sample, while the second laser propagates in a direction perpendicular to that of the first laser and is focused close to the surface of the sample. This laser may or may not form a spark in the environment (air or He) surrounding the sample.

The timing between the two lasers can be chosen so that the ablation laser can either follow or precede the second laser. In the former case, called the *pre-spark mode*, the ablation laser penetrates more easily in the rarified environment created by the second laser, thus interacting more efficiently with the sample surface. In the last case, called the *re-heating mode*, the plasma material created by the ablation laser is further excited by the second laser, thus leading to more efficient excitation-ionization of the plasma constituents. Either way, the signal generated by the double-pulse operation is expected to be greater than that observed with just one laser.

It is worth noting that DP-LIBS has also been used in the *collinear* mode, meaning that the two laser beams propagate to the sample sharing the same optical axis. This way of operation bears the same advantage of the orthogonal scheme regarding the increased ablation-excitation efficiency of the sample. However, it is less versatile, since the pre-spark mode described above is not possible. On the other hand, the collinear scheme is easier to arrange experimentally when stand-off operation is planned.

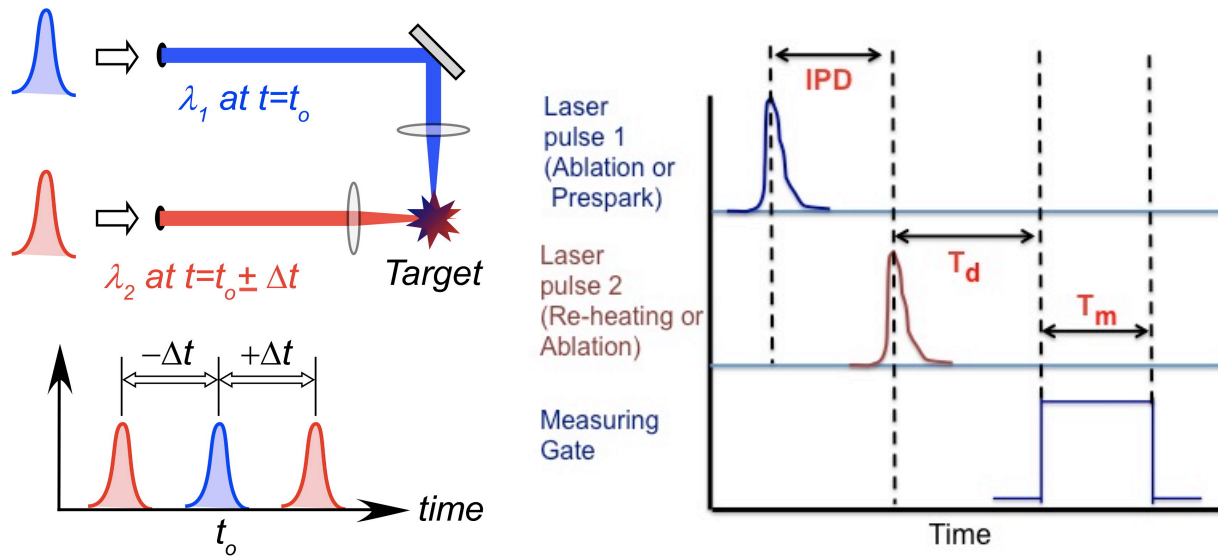


Figure 2-1. Orthogonal double-pulse LIBS operating principle. *Adapted from [3].*

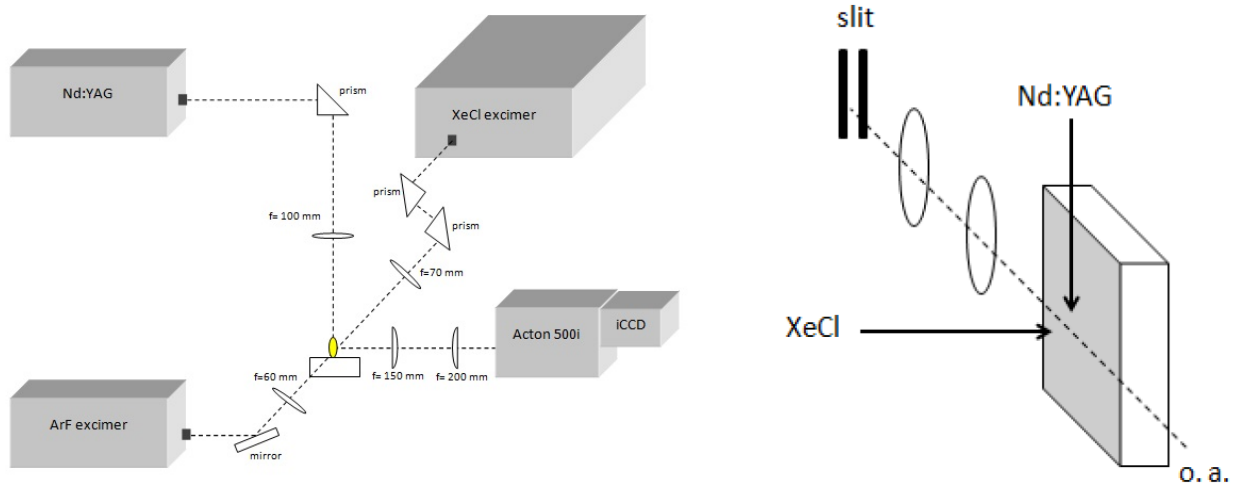


Figure 2-2. Double-pulse orthogonal LIBS experimental setup. o. a.=optical axis.

2.3. Enhancement experiments

The timing diagram is outlined in the right of Fig. 2-1. In double pulse LIBS experiments, there are three time parameters that are important, and in fact characterize the result of the experiment, namely the Inter-pulse Delay time (IPD), the delay of the opening of the gate (T_d) and the gate measuring time (T_m). IPD, T_d and T_m are set by the operator and are continuously variable. In the pre-spark scheme, the gate opens after the ablating laser pulse, while in the re-heating scheme the gate opens after the re-heating pulse. In both cases, the *enhancement* is defined as the *ratio between the signal observed with both lasers to the signal observed with one single laser*.

In order to avoid problems due to sample inhomogeneity and to avoid long, time-consuming accumulation of laser pulses, the *characterization* of the enhancement was carried out with a NaCl window (no longer in use due to previous surface damage). Typical values of the laser energies used were: XeCl: ~100 mJ/pulse; ArF: ~8 mJ/pulse; Nd-YAG: ~300 mJ/pulse.

2.4. Results and discussion

The results of our experiments are reported in Figures 2-3 to 2-8.

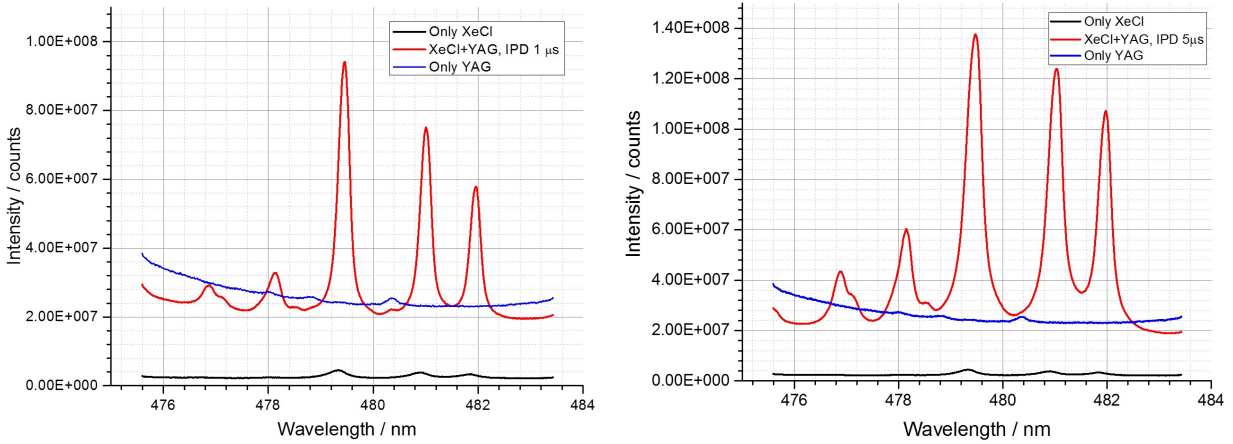


Figure 2-3. *Left*: Experimental enhancement effect observed for an inter-pulse delay (IPD) of 1 μs . *Right*: Same experiment as in the left figure, except for the IPD, which has been set at 5 μs .

Note the strong re-heating effect created by the YAG laser when coupled with the XeCl laser. Note also the increase in the background when the YAG laser is fired. For this experiment, the operating parameters were: XeCl: 112 mJ/pulse; Nd-YAG: 310 mJ/pulse; 10 laser shots accumulated; monochromator slit width: 100 μm ; He environment; $T_m = 1 \mu\text{s}$.

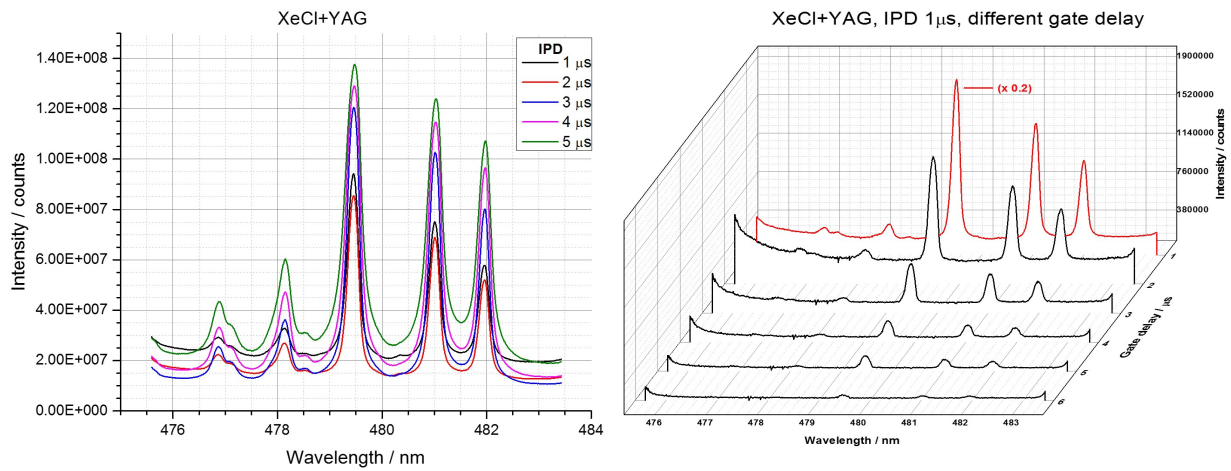


Figure 2-4. Temporal behavior of the enhancement effect due to the re-heating pulse.

The left Fig.2-4 shows the triplet intensity observed at various IPD values from 1 to 5 μs , while Fig. 2-4 right illustrates the signal behavior observed at a *fixed* IPD of 1 μs when the measuring gate was varied from 1 to 6 μs .

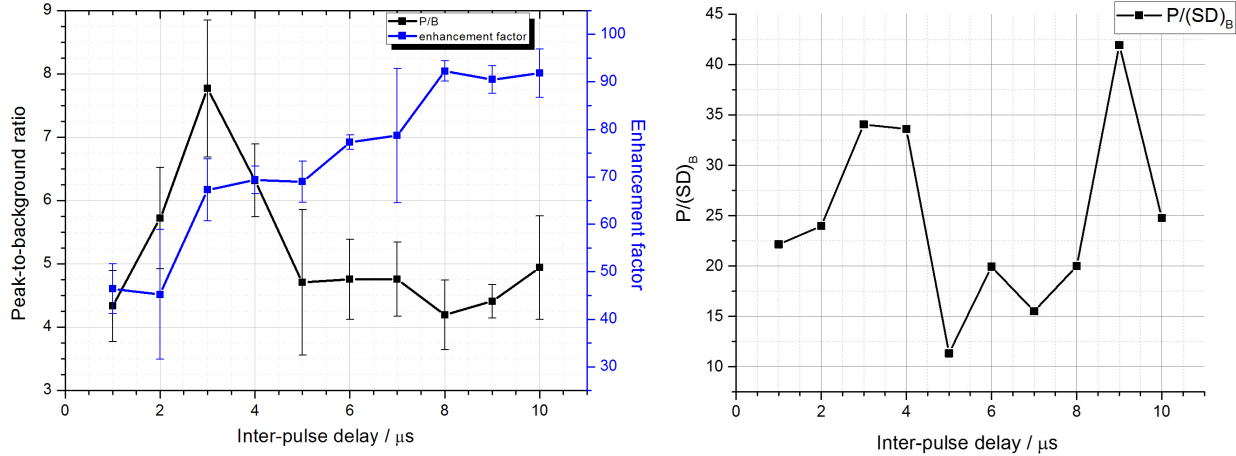


Figure 2-5. *Left*: Net peak signal to background ratio (P/B) and enhancement factor as a function of IPD. *Right*: Temporal behavior of the signal to noise ratio as a function of IPD.

In Fig.2-5, the signal refers to the most intense peak at 479.454 nm. Note that IPD corresponding to the best value of (P/B) does not coincide with that giving the best enhancement. The noise is defined as the standard deviation of the background under the peak. The optimum IPD is found at $\sim 9 \mu\text{s}$.

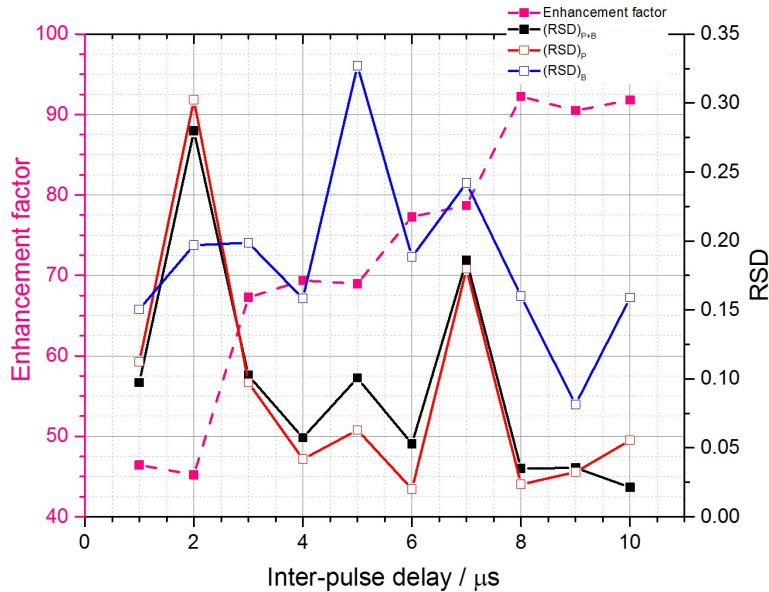


Figure 2-6. Temporal behavior of the RSD of three analytical figures of merit, i.e., P, B, and (P+B), as a function of IPD. The enhancement factor is shown for comparison.

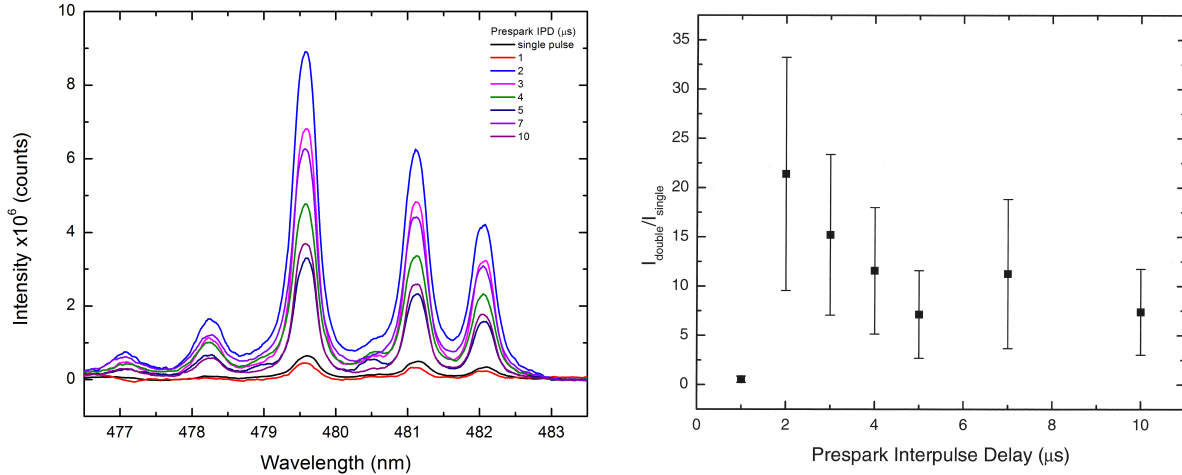


Figure 2-7. *Left:* Temporal behavior of the chlorine triplet observed in the pre-spark mode using two Nd-YAG lasers at 1064 nm. *Right:* Enhancement versus delay.

As shown in Fig. 2-7, one can note that at 1 μs IPD, the enhancement is actually a depression. As expected, the enhancement effect decreases at increasing delays. Operating conditions: Sample: NaCl window; Environment: Air; Ablation laser: Big Sky Ultra, 80 mJ/pulse; Pre-spark laser: Laser Photonics (Model YQL-102+), 180 mJ/pulse.

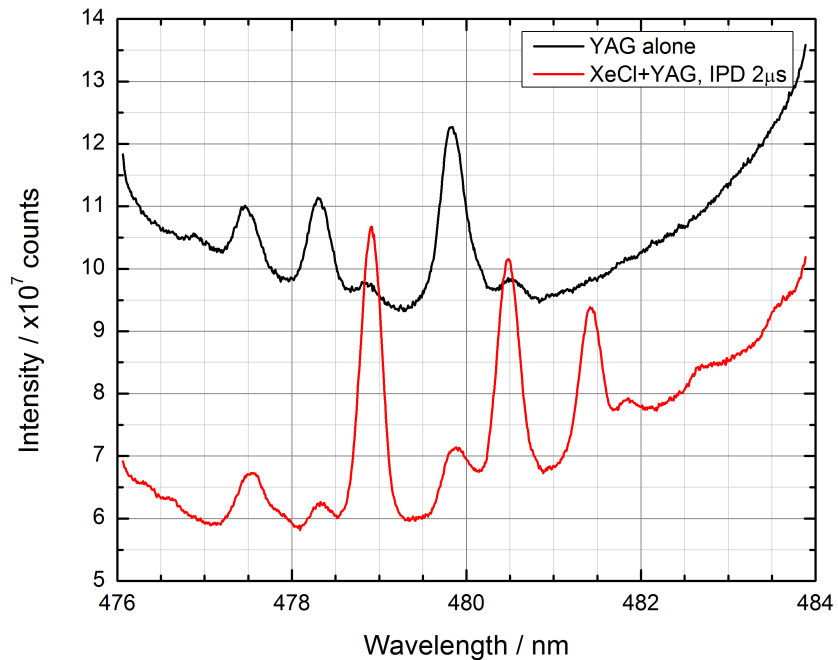


Figure 2-8. Enhancement effect observed in the re-heating mode using the combination XeCl/Nd-YAG lasers.

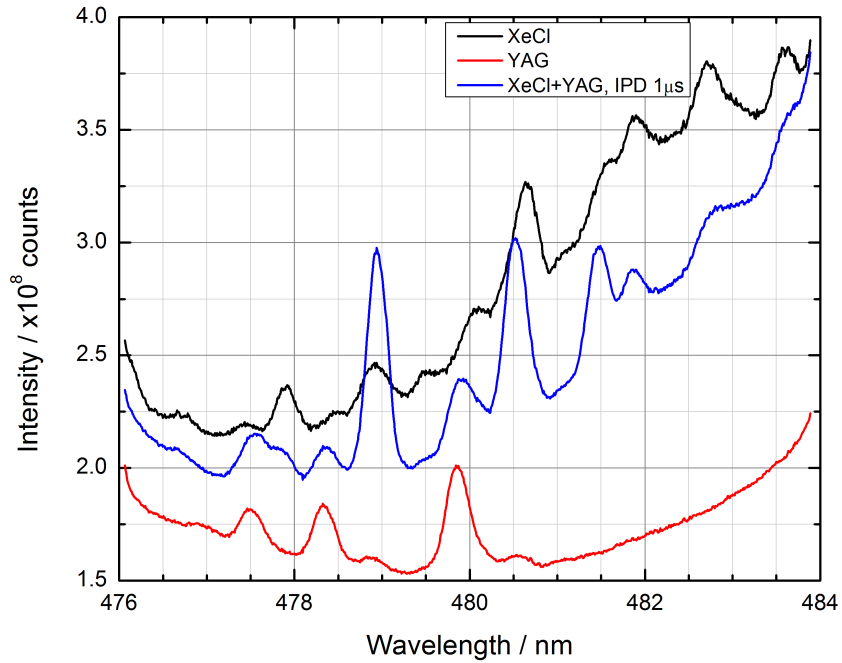


Figure 2-9. Same as figure 2-8, except that here the spectrum obtained with the XeCl laser alone is shown (black trace) and the IPD has been set to 1.0 μ s.

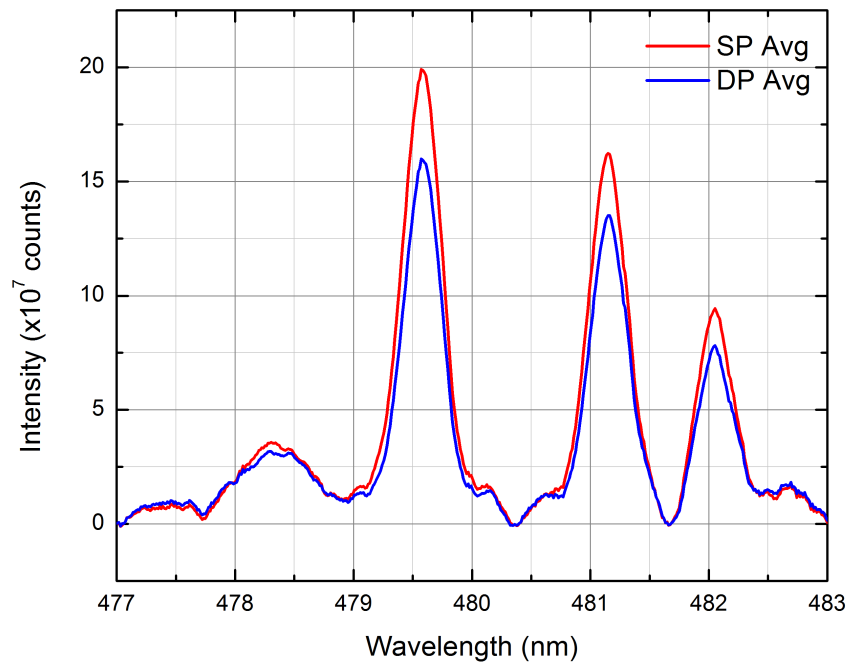


Figure 2-10. Comparison between single-pulse and double-pulse spectra obtained in the pre-spark mode with YAG/YAG combination.

We give here some more operating details regarding Figures 2-8 through 2-10.

The red trace in Fig.2-8 shows the spectrum obtained when the ablation laser is blocked and only the re-heating laser is operated. The sample used was an FDOT 3% Cl, and the laser energies were 108 mJ/pulse for the XeCl laser and 300 mJ/pulse for the YAG laser. $T_g = 0.3 \mu\text{s}$ and $T_m = 2.0 \mu\text{s}$.

The spectra overlaid on the most intense chlorine peak in Fig. 2-9 show an enhancement factor of 5 when the black and blue traces are compared. As in figure 2-8, the combined operation is characterized by a high signal to background noise ratio. The three peaks shown in the YAG spectrum alone (red trace) occurring at 477.97, 478.81 and 480.33 nm, are identified with ionic transitions of nitrogen.

In Fig.2-10, the operating conditions were the following: YAG ablation laser: 80 mJ; Pre-spark YAG: 180 mJ; IPD= 2.0 μs . He environment; 200 laser shots accumulated. Sample: FDOT 3% Cl. Typical of our results in the pre-spark mode, the double-pulse signal is lower than the single pulse, which was also the case observed in Fig. 2-7.

Overall, from the inspection of all figures, the following conclusions can be summarized:

(i) No results could be obtained when the ablating laser was the ArF. The low energy/pulse of this laser (8 mJ in our case) did not provide sufficient ablated material, even from the NaCl sample, to allow a systematic investigation of the enhancement. Moreover, no results are reported for the XeCl/YAG combination *in the pre-spark mode*: this was due to the difficulty in positioning the YAG beam parallel to the sample surface (see Figure 2-1), but separated far enough from it in order to prevent direct laser contact and therefore signal generation with this laser.

(ii) In all cases involving the XeCl excimer and the YAG laser used in the single-pulse experiments of Chapter 1, *enhancements up to almost two orders of magnitude* for the peak signal of the strongest ionic line were found in the re-heating scheme (see Figures 2-3 and 2-5). The striking difference between these findings and the single-pulse results of Chapter 1 is that, while in the last case the chlorine signal was not detectable after a delay of about 1 μs from the plasma formation, in the double-pulse case the signal could still be measured above the background for inter-pulse delays as large as 10 μs . One plausible explanation is that the XeCl laser ablation leaves behind particulate material that persists long enough to be re-vaporized and ionized by the re-heating YAG pulse. In any case, the key result here is that the chlorine signal is strongly enhanced *only* when *both* lasers are present.

(iii) For a fixed inter-pulse delay of 1 μs , the measuring gate could be delayed to almost 6 μs (i.e., $T_d \sim 6 \mu\text{s}$) and the chlorine triplet still be observed, as shown in the figure 2-4 (right figure). From the *analytical* point of view, this implies that the use of larger gate integration times (T_m) can be beneficial.

(iv) The highest peak to background (P/B) ratio and the highest enhancement *do not occur at the same inter-pulse delay* (see left Figure 2-5). In fact, the maximum enhancement coincides with the minimum (P/B) ratio. On the other hand, the peak to background noise ratio (see right figure 2-5) increases with the inter-pulse delay, as does the enhancement. The choice

of the optimum delay will then be dictated by a careful examination of the plots shown in Figure 2-6, *since it is finally the signal-to-background noise ratio that will determine the achievable limit of detection.*

(v) YAG/YAG results.

With the NaCl sample, both pre-spark and re-heating operation modes were investigated. The experiments were carried out in air instead of He since it was easier to produce a spark in air. The pre-spark results are shown in Figure 2-7 (left and right). One can note here that the background induced by the second laser is less complex than that observed in the re-heating mode: this is due to the fact that, in the re-heating mode, the measuring gate opens right after the second laser pulse, which then excites air constituents (e.g., nitrogen).

There are additional considerations. First, the enhancements are *lower* than those obtained with the XeCl/YAG combination. Second, large error bars are associated with the enhancement: this can be attributed to the shot-to-shot wandering of the spatial location of the spark generated by the second laser, since most experiments were carried out in air instead of He. Another interesting result is that the signal obtained in the pre-spark mode at 1 μ s IPD is smaller than that observed in absence of the spark. A tentative explanation of this decrease could be that the short delay does not allow complete formation of the rarified environment in front of the sample surface. If that is the case, the ablation laser pulse will still be absorbed by the pre-spark plasma, thus resulting in less efficient ablation.

A final caveat is that the results obtained with the NaCl window cannot be directly extrapolated to a different matrix, namely a more complex matrix such as concrete.

2.5. Considerations on the detection limits in concrete samples

There are two important *analytical* considerations to be made when comparing single-pulse and double-pulse operation. The first is that the enhancement observed, no matter how large, cannot be directly extrapolated to calculate a similar improvement in the limit of detection, unless it is experimentally demonstrated that the noise in the signal and background are also not enhanced. The second is that the comparison with the results obtained with single-pulse operation must be done with the *optimized single-pulse operation*, namely with the signal obtained using a single laser under optimum operating conditions of laser energy, gate delay and integration time. In other words, it would be misleading to compare the detection limit using the signal obtained with the XeCl laser alone (black trace in Figure 2-3) with that obtained by the XeCl and YAG lasers acting together (red trace in Figure 2-3).

To demonstrate the last point, Figure 2-8 shows the double-pulse signal obtained by ablating a concrete sample containing 3% of Cl (red trace) and the background generated by the YAG laser alone (black trace). The data were obtained using an accumulation of 200 laser pulses on different locations of the sample and firing the re-heating laser 2 μ s after the ablation with the XeCl laser. There is no doubt that the signal-to-noise ratio shown is very high. For a S/N ratio of 3, which is used in the definition of the limit of detection, one can calculate such limit to be in the range 0.05-0.1% Cl. Note that the ablating laser has an energy of 108 mJ/pulse and that the

re-heating laser was operated at 300 mJ/pulse. Similar results were obtained by changing the IPD to 1 μ s, as reported in Figure 2-9. Here, the trace obtained with the ablation laser alone is also reported, showing that a 5-fold enhancement was obtained with both lasers.

The same experiment was repeated with the YAG/YAG combination using He to compare the results of Chapter 1 in a consistent manner. Figure 2-10 shows that no enhancement was observed, confirming that the spark produced by the 180 mJ/pulse YAG laser does not re-excite significantly the material ablated by the 80 mJ/pulse YAG laser.

Finally, we recall that the spectrum reported in Fig.1-11 (Chapter 1) for a chlorine concentration of 0.3% shows that *optimized* single pulse operation provides a limit of detection of 0.04%.

2.6. Conclusions

(i) The ArF energy was too low to generate enough material ablated from the sample surface (in the vapor or particulate phases) to benefit from the further excitation-ionization performed by the second laser.

(ii) The best results were obtained with the XeCl laser as the ablation laser (~100 mJ/pulse) and the high energy (310 mJ/pulse) YAG laser in the re-heating mode: such double-pulse configuration can indeed provide detection limits equivalent to those calculated with the optimized single-pulse experiment, as reported in Chapter 1. It is worth mentioning that a similar conclusion was reached by Sugiyama et al. [5], who reported the same chlorine LOD as the result of SP- and DP-LIBS experiments.

In view of the above findings, it is fair to conclude that, *in our current experience and with the chlorine line chosen*, the use of double-pulse operation does not offer an advantage significant enough to outweigh the additional complexity of adding another laser to the system, especially in view of a potential “in situ” exploitation.

CHAPTER 3. SINGLE-PULSE LIBS DETECTION OF CHLORINE IN CONCRETE USING CaCl EMISSION

3.1: Literature survey

Normally, molecular spectra are not expected to be strong in the high temperature plasma induced by laser, in view of the fact that the high temperature dissociates the molecular species present in the plasma. On the other hand, both temperature and electron number density decay during the time evolution of the plasma and molecular emission of many species can be indeed been observed at suitable delays after the firing of the laser ablation pulse [3,41]. Most interesting, the possibility of isotopic molecular analysis is now well documented [42]. Molecular emission using LIBS plasmas is then becoming a popular and promising way of detecting molecular species and quantifying their constituents atoms.

With specific reference to halogen detection, high-resolution *absorption* spectroscopy with a continuum source has been proposed as a sensitive detection technique of halogens in different atom reservoirs using AlCl and SrCl [43-46]. Gaft et al. [47] have pointed out that fluorine and chlorine combine with alkali-earths and other elements to form molecules whose spectra may be easily identified, enabling detection in ambient conditions with much higher sensitivity than using F and Cl atomic lines. The determination of fluorite mass-content in powdered ores using CaF emission has also been recently reported [48].

In the *framework of this project*, namely the detection of chlorine in concrete samples, the full potential of molecular sensing schemes has not yet been realized. In view of the high concentration of Ca in cement, it would seem logical to study the feasibility of detecting the emission of CaCl and assess the sensitivity of the approach. Forni et al. [49] reported the first observation of CaF and CaCl emission with the CHEMCAM instrument on board the Mars Science Laboratory, but no quantitative data were given. The first quantitative analytical data using LIBS emission of CaCl in cement was reported by Guenther et al. [50] in a poster presentation at the EMSLIBS symposium in 2015, and later by us [51] in a more recent poster presentation at the Pittcon conference this year. Guenther et al. [50] reported a limit of detection for Cl of 0.03%, using the molecular emission of CaCl at 593 nm.

At present, to our knowledge, the above two studies are the only analytical studies of CaCl emission in concrete samples. The band chosen for our investigation (593.5 nm) has been exhaustively investigated in the literature [52-55]. These papers are of fundamental interest for the spectroscopic characterization of the molecule (e.g., vibro-rotational molecular level assignments, isotope resolution, excited state lifetimes) rather than for its analytical detection.

3.2: Setup of molecular LIBS instrumentation

The present results were obtained with the same set-up already described in Chapters 1 and 2. In fact, no modifications are necessary to switch from the detection of chlorine ionic emission to molecular CaCl emission. The same holds for the detection and data processing system. Both gratings (1200 grooves/mm and 2400 grooves/mm) were used interchangeably, since the increased resolution was advantageous in the discrimination of the background from

the analytical signal. Contrary to the case of Cl ionic emission (see Chapter 1) where a He environment was always used, molecular detection was measured both in air and He.

3.3. Single-pulse molecular LIBS experiments

CaCl has three extensive systems with band heads at 621.39 nm, 593.47 nm and 377.39 nm [52]. We have first reproduced the low resolution LIBS CaCl spectral data obtained by Gaft et al. [47]. The most prominent CaCl bands observed occur at 593.5 nm, 606.9 nm, 618.8 nm and 631.4 nm. Other bands were observed in the UV region but were plagued with spectral interference from strong Ca ion emission. All the experiments were then performed at 593.5 nm. Other emissions from molecules like CuCl, SiCl and AlCl were either not observed or their emission intensity was not comparable to that of CaCl. As before, the samples used were provided by FDOT (Gainesville) and by BAM (Berlin, Germany).

The results of our experiments are reported in Figures 3-1 to 3-8 and the analytical calibration curves obtained and used for the calculation of the limit of detection are shown in Figures 3-9 and 3-10.

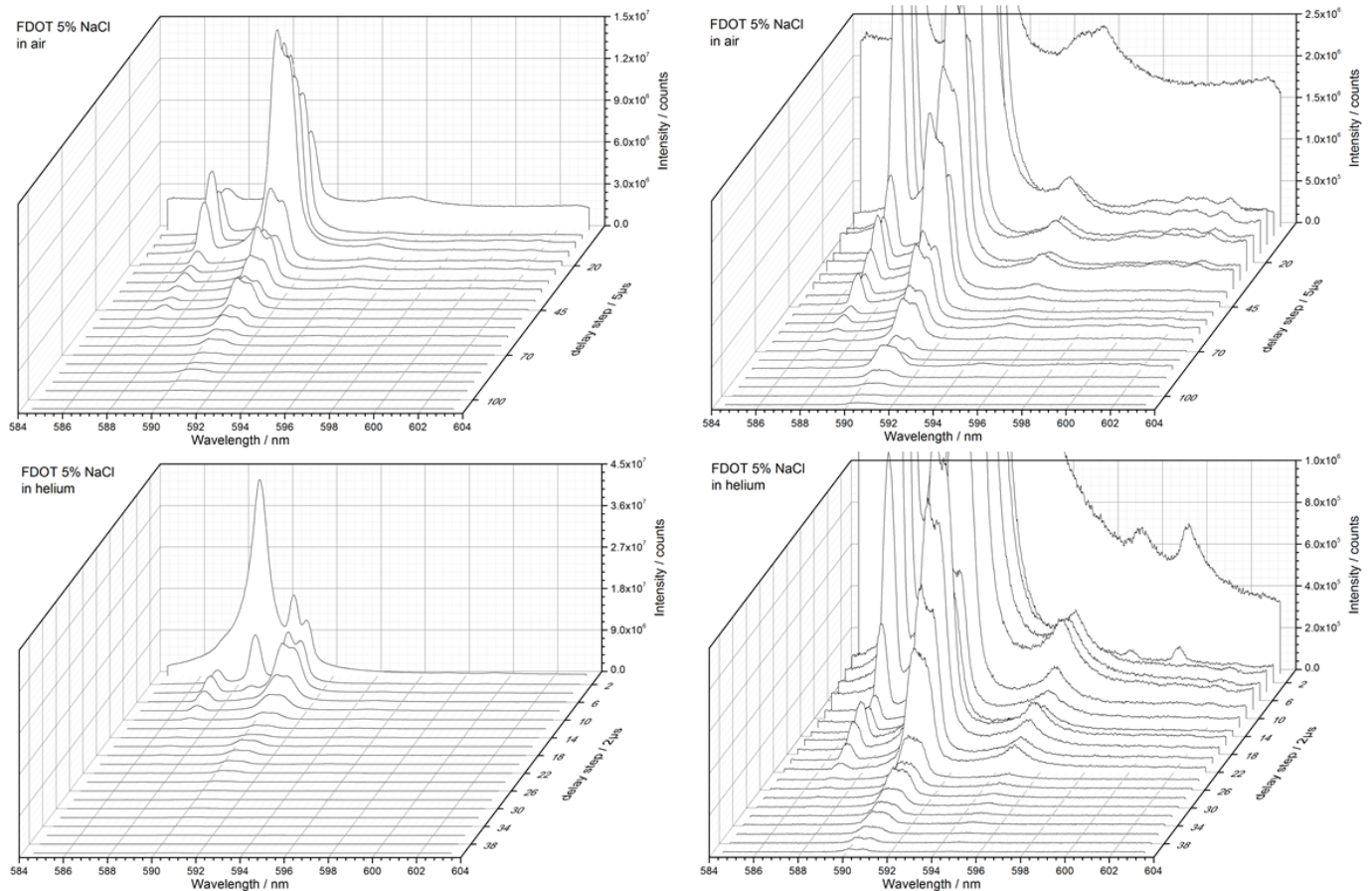


Figure 3-1. Temporal evolution of the CaCl band at 593.5 nm taken with the 1,200 gr/mm grating. *Top (left and right): air; Bottom (left and right): He. Sample: FDOT 3% Cl.*

Figure 3-1 illustrates the temporal evolution of the spectral region encompassing the CaCl band at 593.5 nm taken with a low resolution grating (1200 grooves/mm). Measurement conditions: laser energy: 250 mJ/pulse; repetition rate: 1 Hz; gate width: 1.0 μs ; monochromator slit width: 100 μs , ICCD Gain: 250. Figures on the right are intensity-expanded as well as time-expanded views to better appreciate the CaCl features. The very high background observed at zero delay is typical of LIBS plasmas and the broad feature is due to nitrogen emission, which is seen to a lesser extent when He replaces air. The other spectral features are due to Na and Ca emission lines in air and He, with the addition of a He line when He replaces air.

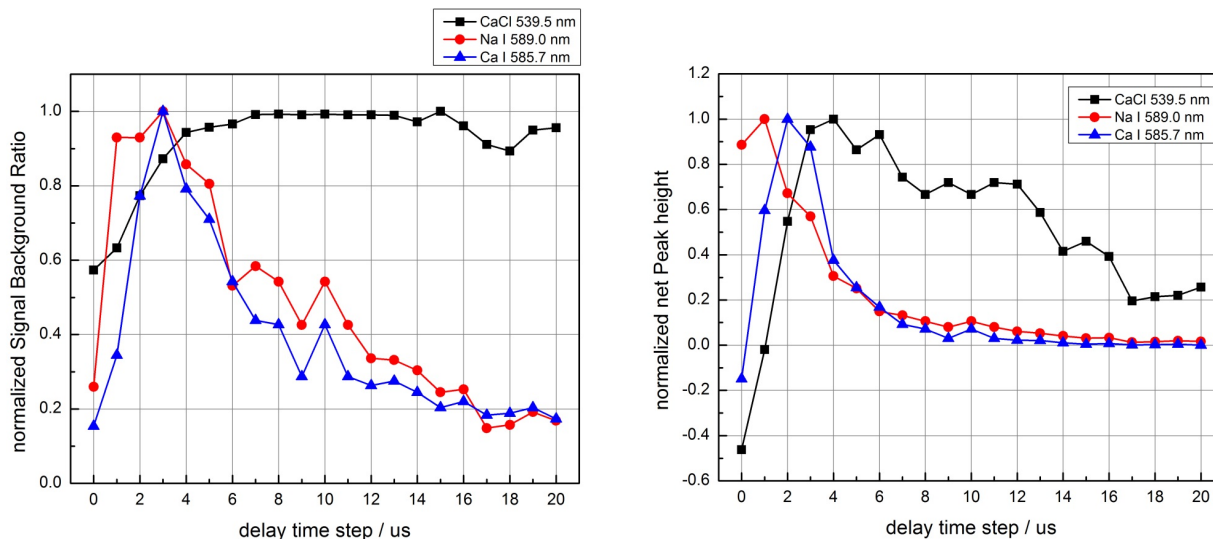


Figure 3-2. Temporal evolution of the signal-to-background ratio (S/B) (*left*) and net signals (*right*) relative to molecular and atomic emission of CaCl, Na, and Ca.

In analogy to Figure 3-1, Figure 3-2 illustrates the time behavior of molecular CaCl emission as well as that of Na and Ca atoms. As expected, both atomic signals and background decrease more rapidly than molecular emission, while the S/B ratio of CaCl emission increases up to about 6 μs delay time and then remains relatively constant. It is also interesting to note that molecular emission starts early in the plasma evolution.

The above figure emphasizes the importance of obtaining experimental time-decay information of species relevant to formation of the emitting molecule: such information will allow choosing the right delay and integration times for the optimization of the signal to background ratio (see Figure 3-5).

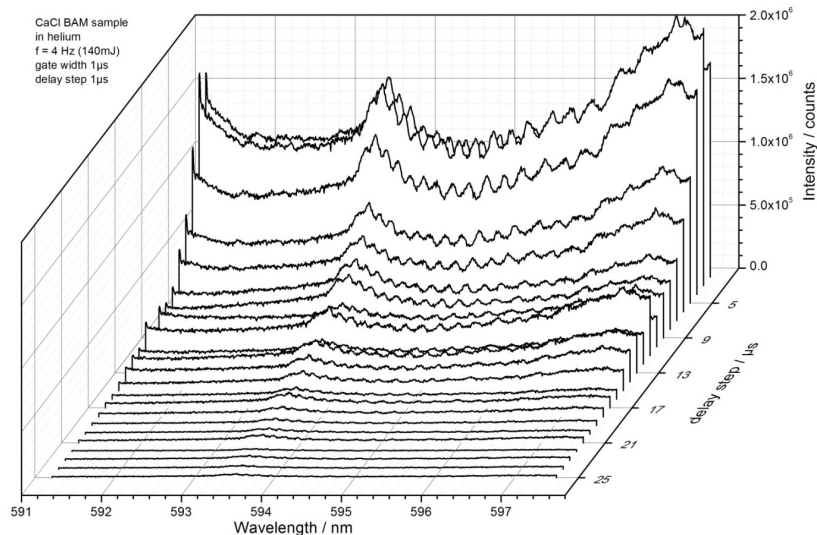


Figure 3-3. Temporal evolution of the CaCl band emission in He. Sample: BAM 2.26% Cl.

Figure 3-3 illustrates the detailed temporal evolution (1 μs delay, 1 μs integration time) of the CaCl band emission observed at moderately high spectral resolution (note the total spectral window of about 6 nm) in a He environment. Here, the typical vibronic features of molecular emission are clearly seen. The background at the right hand side is limited by CaO emission and on the left hand side by the strong sodium atomic emission. From an analytical point of view, the correction of the background constitutes the most challenging problem. The measurements were taken with a laser energy of 140 mJ/pulse.

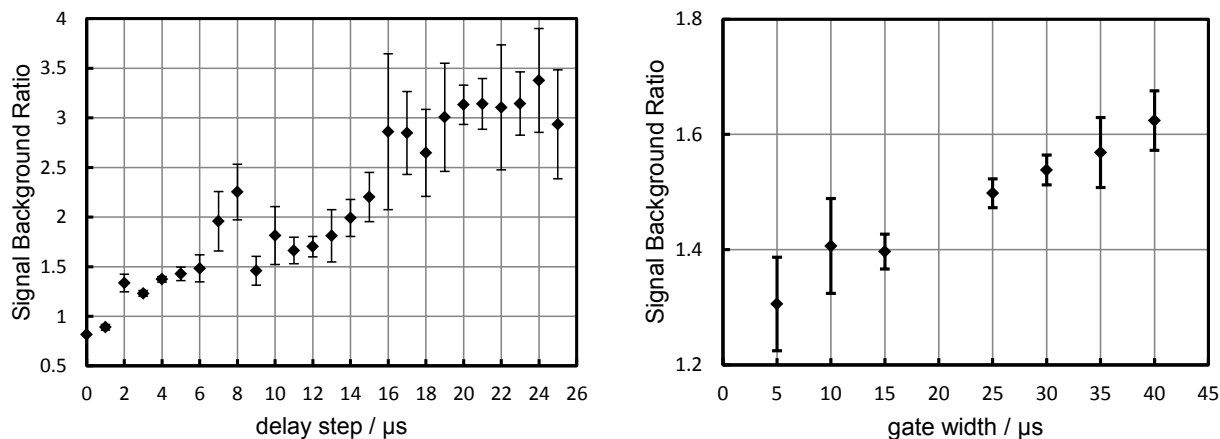


Figure 3-4. Analytical behavior of the signal-to-background ratio as a function of the gate delay (*left*) and gate integration time (*right*).

By using the time-resolved data reported in the previous figures, one can optimize the analytical Signal-to-Background ratio by choosing the best gate delay and integration time. In agreement with the results shown in figures 3-2 and 3-3, the S/B ratio improves as the delay increases (stabilizing around 18 μs) and as the integration time increases. Depending upon the environment (air or He), even higher integration times (up to 80 μs) can be used.

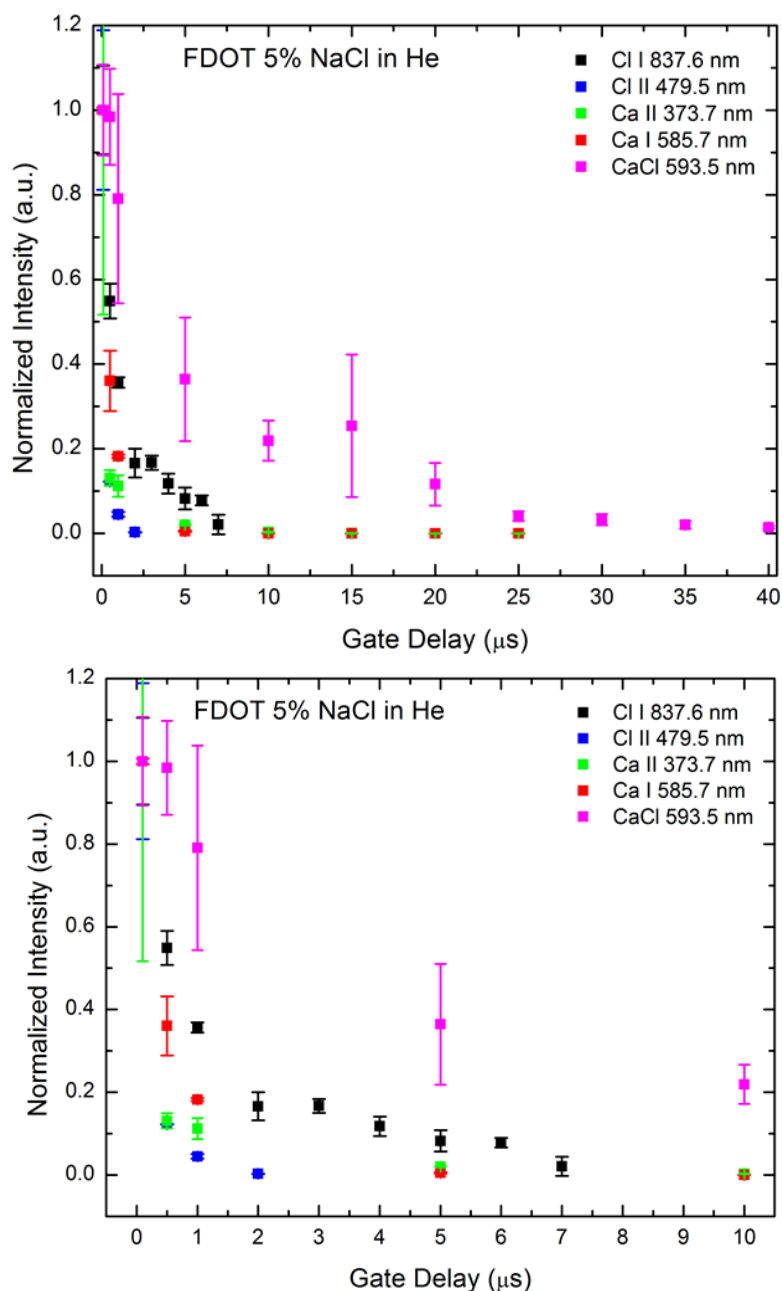


Figure 3-5. Temporal behavior of several species relevant to the kinetics of formation of CaCl in the plasma, as indicated in the x-axis.

The temporal behavior of atomic, ionic, and molecular emission of Cl and Ca are shown in Figure 3-5. The species chosen are assumed to be relevant to the kinetics of formation of the CaCl molecule. Note the shorter persistence of atomic and ionic chlorine line emission in comparison with that of the CaCl band. Moreover, the ionic calcium line emission persists significantly less than the atomic calcium emission.

A detailed modeling of the kinetics of all the species involved as well as of the chemical reactions occurring in the plasma would be needed before attempting to explain the formation and persistence of the CaCl molecule. However interesting and necessary, such effort was considered out of the scope of the present project.

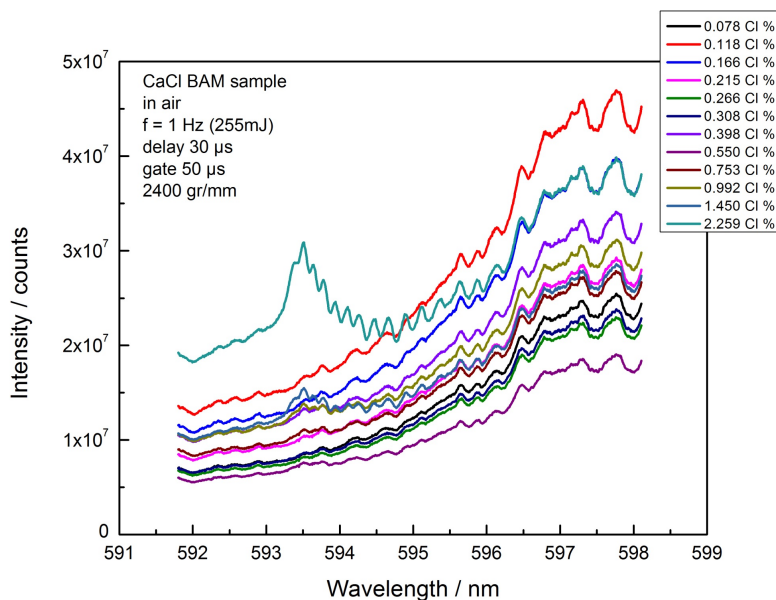


Figure 3-6. Analytical signals obtained at different chlorine concentration concentrations in the low percent range, as indicated in the box.

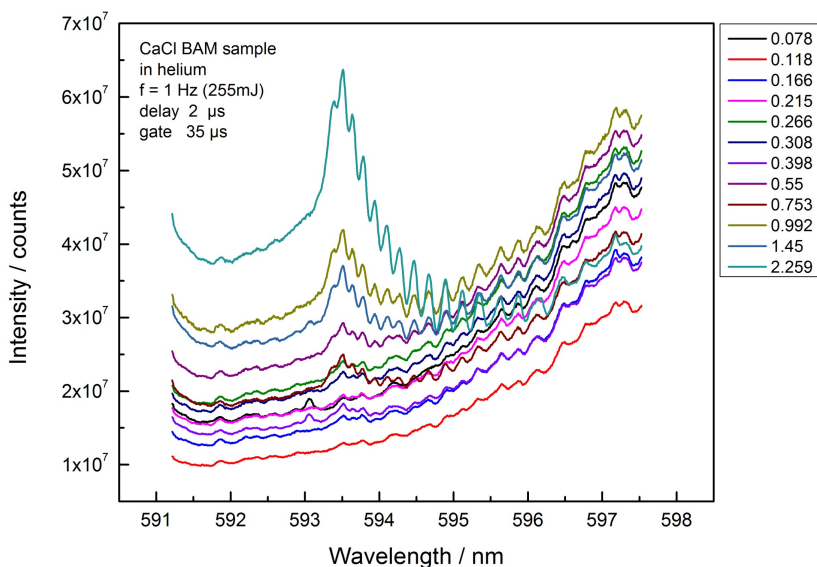


Figure 3-7. Same as figure 3-6, except that the experiment was performed in a He atmosphere.

The spectral features of the CaCl emission band at different low Cl concentrations are collected in Figures 3-6 (air environment) and 3-7 (He environment). The gate delay and integration times are indicated in the inset (note the different delays used). The measurements performed in air show strong spectral features of CaO emission, whose formation is due both to the air environment and to the sample constituents (e.g., CaCO₃). Indeed, as seen in Figure 3-7, despite the He environment, CaO emission is still visible. The present of this spectrally structured band constitutes the main challenge to background correction on the high wavelength side of the emission peak.

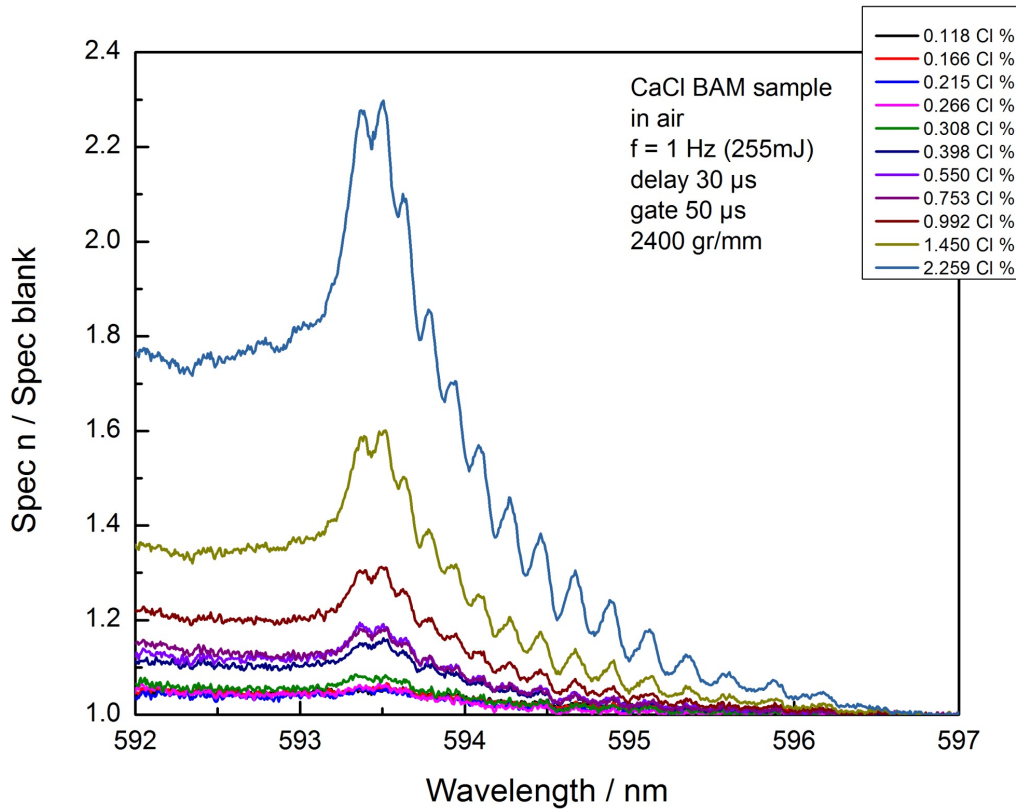


Figure 3-8. Analytical improvement resulting from normalizing (pixel by pixel) the spectra for various sample concentrations to the lowest concentration spectrum (assumed equivalent to a *blank* spectrum).

Figure 3-8 shows the significant analytical improvement resulting from ratioing (pixel by pixel), in the spectral interval of figure 3-6, the intensities obtained with the various sample concentrations (indicated as *Spec n* in the Y-axis) to those given by the lowest concentration (assumed equivalent to a blank spectrum, and thus indicated as *Spec-blank*). The outcome of this mathematical approach results in a much more reliable estimate of the background of the high-wavelength side of the peak.

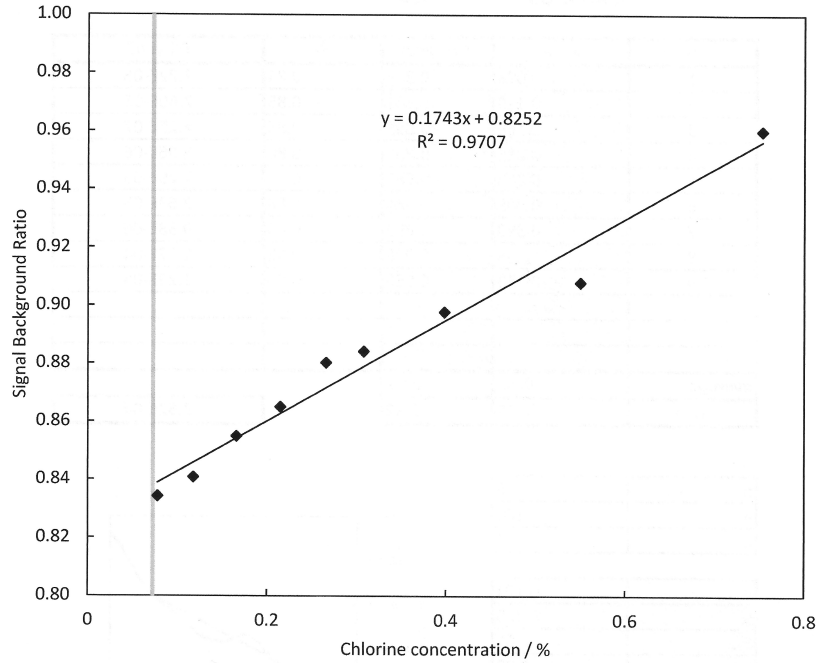


Figure 3-9. Calibration curve obtained in the ambient air by plotting the S/B ratio as a function of Cl concentration in the range 0.08-1% Cl.

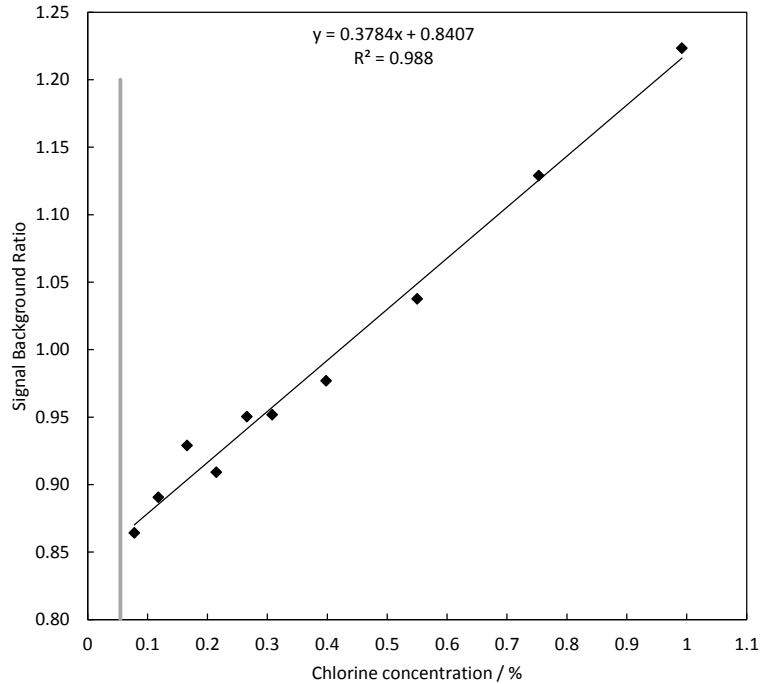


Figure 3-10. Calibration curve obtained in the He environment by plotting the S/B ratio as a function of Cl concentration in the range 0.08-1% Cl.

Figures 3-9 and 3-10 report the calibration curves obtained in the ambient air and He by plotting the S/B ratio as a function of Cl concentration in the range 0.08-1% Cl. The experimental conditions, namely laser energy, gate delay and gate integration time, were identical to those reported in figures 3-8 and 3-9. The limit of detection (LOD), calculated (using the standard DIN 32645 protocol) was 0.07% Cl in air and 0.05% in He.

In conclusion, from all the figures shown in this Chapter 3, we can summarize the following analytical information:

(i) The temporal persistence of the various emission spectral features in air is longer than that observed in He. In addition, the strong emission due to sodium at 590 nm makes it difficult to evaluate the *net signal peak* due to CaCl. This is particularly evident in the two top right spectra of Figure 3-1. Another observation is that, contrary to common expectation, CaCl forms very early in the plasma, when the temperature is high, indicating that the molecule is chemically stable.

(ii). The Signal-to Background ratio increases when the delay increases and when the integration time increases. This is consistent with the time behavior of both signal and background. Indeed, as seen in Figure 3-5, the time decay of four relevant species, namely Cl, Cl⁺, Ca, Ca⁺, is faster than CaCl.

(iii). The limit of detection, calculated using the standard DIN 32645 protocol (see Chapter 1) was found to be marginally better in He (0.05%) than in air (0.07%). For this calculation, each data set is the result of 100 laser shots (20 laser shots accumulated at a given sample location and five different locations ablated for each sample).

3.4. Considerations on the detection limits in concrete samples

The same considerations given in Chapter 1 are valid here: the limiting Cl value for rejection (*corrosion limit*) communicated by FDOT (~200 ppm or~ 0.02%) is practically the same as our detection limit and therefore cannot be quantified. Again, however, other limits, such as *critical content* or *critical threshold* values are reported to be in the range 0.2-0.4%. Our present results using CaCl molecular emission indicate that these critical values can be reliably quantified (see figures 1-10 and 1-11).

3.5. Conclusions

(i) Our study has confirmed that the use of CaCl emission in the plasma can be analytically *as good as* the use of atomic and/or ionic emission of chlorine. We have assumed that excess of Ca with respect to Cl should assure that the molecular emission is linearly dependent upon the chlorine concentration in the entire range of chlorine concentrations investigated. However, we have not investigated this quantitative aspect either theoretically or with an *ad hoc* experiment.

(ii) Our study has confirmed that an experimental knowledge of the *temporal evolution* of different species in the plasma is necessary in order to optimize the detection in terms of signal, background and data acquisition parameters.

(iii) It has been demonstrated that the choice of the optimum gate delay and gate integration time allow reliable detection and quantitation of chlorine in concrete at the 0.2% level, with a limit of detection of 0.05% in He and 0.07% in air.

In view of the above findings, it is fair to conclude that, in our current experience and with the present set-up, molecular emission of CaCl at 593.5 nm *is a welcome addition* to the use of the atomic ion chlorine line at 479.5 nm (our work) and the atomic neutral chlorine line at 837.6 nm (mostly used in the literature). Compared to the results obtained with the ion line, molecular emission presents the *distinct advantage* that the analytical measurements can be performed at an optimum delay after plasma formation, rather than at “zero” delay like in the case of 479.5 nm measurements, where the zero delay was necessary in view of the short persistence ($\sim 1 \mu\text{s}$) of the analytical Cl ion signal.

CHAPTER 4. OVERALL CONCLUSIONS AND ANALYTICAL CONSIDERATIONS

4.1. Definitions of critical chlorine values in concrete and their relevance to this report

In the three previous chapters, reference is often made to terms like “corrosion threshold” and “critical chloride content”. These terms are obviously important reference criteria to be taken into account when evaluating the analytical performance of the methodology developed. Understanding this terminology implies specific knowledge of the causes of degradation of reinforced concrete structures due to harmful environmental agents (chlorine being one of them) and on the time scale in which such degradation reaches the point where repairing and other more drastic actions need to be taken. Chemical analysis of building material is therefore a complex problem of civil engineering, requiring multiple expertise in material science, corrosion science and analytical instrumentation.

The definitions of the above terms are quoted here from a literature review by Virmani and Ghasemi [56] made in support of a laboratory study on corrosion of grouted post-tensioned tendons affected by chloride contamination. In this review, the *allowable chloride limit* is quoted as “the maximum amount of chloride in fresh concrete permitted by a code authority”. On the other hand, a *chloride threshold* is an actual chloride concentration causing corrosion initiation of a passivated (i.e., immune from corrosion) metal embedded in concrete and grout. The *chloride threshold value* is also called *critical chloride content*. In general, preset chloride limits are lower than experimentally determined chloride threshold values [56].

Still quoting Virmani and Ghasemi [56], “corrosion initiates when the protective oxide film is compromised at and above a chloride concentration value, namely the *chloride threshold value*, or by carbonation (lowering pH). For chloride-induced corrosion, it is desirable to have a reliable chloride threshold value to predict when corrosion can initiate on metals embedded in a particular cementitious material.”

The review [56] makes also clear the distinction between *acid-soluble chloride* and *water-soluble chloride*. The former concentration “represents the total content of chloride, and includes all chloride ions that are potentially available for future corrosion in the concrete and grout matrix”. The last concentration, also referred to as the amount of free chloride ions, is “the amount of chloride ions dissolved in concrete, grout, or cementitious materials available for corrosion at the moment of analysis”.

Finally, the review report a useful collection of several published total chloride threshold values in samples of mortar, concrete and grout. Their Table 2 is reproduced here (Table 4-3).

Table 4-3. Review of total chloride threshold values in mortar, grout and concrete. From reference 56.

Table 2. Published total chloride threshold values relevant to this literature review.						
No.	Researchers (Year)	Published Total Chloride Threshold Values (Percent by Weight of Cement)		Testing Medium	Material	Reference No.
		Max	Min			
1	Elsener and Bohmi (1986)	0.5	0.25	Mortar	Sandblasted bar	23, 27
2	Hansson and Sorensen (1990)	1.6	0.4	Mortar	Unknown	18, 23
3	Alonso et al. (2000)	3.08	1.24	Mortar	Rebar and smooth bar	27
4	Zimmermann et al. (2000)	1.25	0.25	Mortar	Unknown	27
5	Trejo and Pilai (2003)	0.24	0.04	Mortar	Cleaned/degreased bar	27
6	Trejo and Monteiro (2005)	0.15	0.05	Mortar	Mill scaled bar	27
7	Sagues et al. (2005)	0.08 by a conversion factor of 1.493 from grout weight to cement weight		Grout recharged with fresh water	7-wire strand	25
8	Azuma et al. (2007)	1.2	0.035	Grout		26
9	Trejo et al. (2009)	0.018	0.006	Grout		28, 29
10	Stark (1984)	0.17 ^a	0.11 ^a	Concrete		35
11	Pfeifer et al. (1987)	1.4	1.2	Concrete		20, 21
12	Stratful et al. (1975)	1.4	0.17	Concrete		Unknown
13	Clear (1976)	0.2		Concrete	Rebar	20
14	Locke and Siman (1980)	0.8	0.4	Concrete	Rebar and cleaned bar	27 ^b
15	Vassie (1984)	1.5	0.2	Concrete	Unknown	18, 23
16	Lukas (1985)	2.2	1.8	Concrete	Unknown	18, 23
17	Hope and Ip (1987)	0.19	0.1	Concrete	Polished bar	27
18	Pfeifer et al. (1987)	0.26	0.17	Concrete	Rebar	20, 21
19	Treadaway et al. (1989)	1.9	0.32	Concrete	Unknown	18, 23
20	Schiesl and Raupach (1990)	2	0.5	Concrete	Unknown	18, 23
21	Thomas et al. (1990)	0.5		Concrete	Unknown	18, 23
22	Lambert et al. (1991)	2.5	1.6	Concrete	Unknown	18, 23
23	Tuuti (1993)	1.4	0.5	Concrete	Unknown	23
24	Henriksen (1993)	0.7	0.3	Concrete	Unknown	18, 23
25	Bamforth and Chapman-Andrews (1994)	0.4		Concrete	Unknown	18, 23
26	Thomas (1996)	0.7	0.5	Concrete	Unknown	18, 23
27	Morris et al. (2004)	1.3	0.4	Concrete	Unknown	27
28	Nygard and Geiker (2005)	0.75	0.52	Concrete	Smooth bar	27
29	Manera et al. (2008)	2	1.1	Concrete	Rebar and smooth bar	27

^a Water-soluble chloride.

^b Mean value of 0.6 reported in references 18 and 23.

For our purposes, taking into account that the values are referred to percent weight of total chloride in cement, it is interesting to see that the critical values quoted encompass a large range, between a minimum of 0.006% (grout) to a maximum of 3.08% (mortar). For concrete samples, the values vary in the range from 0.11% (water soluble Cl) to 2.5%. Except for the minimum chlorine value in the grout, the limits of detection and quantification reported in Chapters 1-3 are well within the range of values tabulated.

4.2. “In situ” and “stand-off” LIBS

The title of this report includes explicitly the words “in situ” feasibility of the LIBS approach proposed. Indeed, one unique feature of LIBS is its inherent capability of remotely addressing the sample and collecting the resulting plasma photons for analysis with little or no sample preparation. The “no sample preparation” of LIBS has indeed become a cliché [3].

For the specific analysis of chlorine in construction materials, portable LIBS and stand-off LIBS operation have been recently described in the literature [57-59]. At BAM (Berlin, Germany), a mobile LIBS system is being developed for on-site application on building structures and parking decks [58]. Another group in Japan [59] has described remote (5 m) chlorine measurement of sea salt attached to stainless steel located at the sidewall of a narrow gap (~50 mm). These works are usually accompanied by measurements of the penetration profiles of chlorine in concrete structures [60-66]: normally, these studies are performed on samples taken from the investigated structure and brought into the laboratory.

All the measurements performed in our laboratory can be described as “in situ” measurements, in the sense that no sample preparation was involved prior to the LIBS measurements. The measurements are obviously not stand-off, since the sample was not analyzed in field. Taking into account the calibration sensitivity obtained, we conclude that collecting the sample at the damaged structure and providing an accurate, highly resolved spatial profile of the chloride penetration by cutting the sample in the laboratory would be the best way to proceed for corrosion studies. Several of the listed references describe the use of LIBS to provide *detailed depth profiles*, with spatial resolutions of 1 mm [see, e.g., 14, 20, 61, 62] and imaging of the element distribution, all of this in a much faster time and assessing a relatively large surface area (~100 cm²) compared to micro-scanning techniques. In addition, the *carbonation depth* of the concrete can also be estimated.

In a laboratory already routinely involved in quantifying chlorine in concrete by wet chemistry methods or using X-ray Fluorescence, LIBS will add substantially to its overall analytical performance.

REFERENCES

1. R. Noll, *Laser Induced Breakdown Spectroscopy*, Springer-Verlag, Berlin (2012).
2. D.W. Hahn and N. Omenetto, LIBS, “Part I: Review of basic diagnostics and plasma-particle interactions: Still-challenging issue within the analytical plasma community”, *Appl. Spectrosc.*, 64, 336A-366A (2010).
3. D.W. Hahn and N. Omenetto, “LIBS, Part II: Review of instrumental and methodological approaches to material analysis and applications to different fields”, *Appl. Spectrosc.*, 66, 347-419 (2012).
4. V.S. Burakov, V.V. Kiris, and S. N. Raikov, “Optimization of conditions for spectral determination of chlorine content in cement-based materials”, *Journal of Applied Spectroscopy*, 74(3), 321-327 (2007).
5. K. Sugiyama, T. Fujii, T. Matsumura, Y. Shiogama, M. Yamaguchi and K. Nemoto, “Detection of chlorine with concentration of 0.18 kg/m³ in concrete by laser-induced breakdown spectroscopy”, *Appl. Opt.*, 49, C181-C190 (2010).
6. T. A. Labutin, A. M. Popov, S. N. Raikov, S. M. Zaytsoev, N. A. Labutin, and N. B. Zorova, “Determination of chlorine in concrete by laser-induced breakdown spectroscopy in air”, *Journal of Applied Spectroscopy*, 80(3), 315-318 (2013).
7. C. Haisch, R. Niessner, O. I. Matveev, U. Panne and N. Omenetto, “Element-specific determination of chlorine in gases by Laser-Induced-Breakdown-Spectroscopy (LIBS)”, *Fresenius J. Anal. Chem.*, 356, 21-26 (1996).
8. N. Silva, T. Luping and S. Rauch, “Application of LA-ICP-MS for meso-scale chloride profiling in concrete”, *Materials and Structures* 46, 1369–1381 (2013).
9. N. Watanabe, W. Buscher and G. Bohm, “Determination of F, Cl, Br and I by barrier discharge radiofrequency He plasma”, *Anal. Sciences* 18, 1191-1194 (2002).
10. T. Jacksier and R.M. Barnes, “Atomic emission of chlorine: Spectra from 200 to 900 nm by sealed ICP-AES”, *Appl. Spectrosc.* 48(3), 382-386(1994).
11. Peter C. Taylor, Ezgi Yurdakul, Halil Ceylan, “Concrete pavement mixture design and analysis (MDA): Application of a portable X-ray fluorescence technique to assess concrete mix proportions”, A report from National Concrete Pavement Technology Center, Iowa State University, March 2012.
12. F. Weritz, D. Schaurich . A. Taffe . G. Wilsch, “Effect of heterogeneity on the quantitative determination of trace elements in concrete”, *Anal. Bioanal. Chem.*, 385, 248–255 (2006).
13. F. Weritz, D. Schaurich, G. Wilsch, “Detector comparison for sulfur and chlorine detection with laser induced breakdown spectroscopy in the near-infrared-region”, *Spectrochim. Acta Part B*, 62, 1504–1511 (2007).
14. F. Weritz, A. Taffe, D. Schaurich, G. Wilsch, “Detailed depth profiles of sulfate ingress into concrete measured with laser induced breakdown spectroscopy”, *Construction and Building Materials*, 23, 275–283 (2009).
15. M.A. Gondal, M.A. Dastageer, M. Maslehuddin, A.J. Alnehmi, O.S.B. Al-Amoudi, “Detection of chloride in reinforced concrete using a dual pulsed laser-induced breakdown spectrometer system: comparative study of the atomic transition lines of Cl I at 594.85 and 837.59 nm”, *Appl. Opt.*, 50, 3488-3496 (2011).
16. M. A. Gondal, Z. H. Yamani, T. Hussain and O. S. B. Al-Amoudi, “Determination of Chloride Content in Different Types of Cement Using Laser-Induced Breakdown

- Spectroscopy”, *Spectrosc. Lett.*, 42,171–177 (2009).
17. M. A. Gondal, A. Dastageer, M. Maslehuddin, A.J. Alnehmi and O. S. B. Al-Amoudi, “Sensitivity enhancement at 594.8 nm atomic transition of Cl I for chloride detection in the reinforced concrete by LIBS”, *J. Env. Sci. &Health, Part A*, 46, 198-203 (2011).
 18. M. Tran, Q. Sun, B.W. Smith and J.D. Winefordner, “Determination of F, Cl, and Br in solid organic compounds by Laser induced plasma spectroscopy”, *Appl. Spectrosc.*, 55 (6), 739-744 (2001).
 19. G. Asimellis, S. Hamilton, A. Giannoudakos and M. Kompitsas, “Controlled inert gas environment for enhanced chlorine and fluorine detection in the visible and near-infrared by laser-induced breakdown spectroscopy”, *Spectrochim. Acta Part B* 60 (2005) 1132 – 1139.
 20. T. Eichler, B. Isecke, G. Wilsch, S. Goldschmidt and M. Bruns, “Investigations on the chloride migration in consequence of cathodic polarization”, *Materials and Corrosion*, 61(6), 512-517 (2010).
 21. L. Dudragne, Ph. Adam, and J. Amouroux, “Time-Resolved Laser-Induced Breakdown Spectroscopy: Application for Qualitative and Quantitative Detection of Fluorine, Chlorine, Sulfur, and Carbon in Air”, *Appl. Spectrosc.*, 52(10), 1321-1327 (1998).
 22. J.D. Pedarnig, M.J. Haslinger, M.A. Bodea, N. Huber, H. Wolfmeir and J. Heitz, “Sensitive detection of chlorine in iron oxide by single pulse and dual pulse laser-induced breakdown spectroscopy”, *Spectrochim. Acta Part B*, 101, 183-190 (2014).
 23. C.D. Gehlen, E. Wiens, R. Noll, G. Wilsch and K. Reichling, “Chlorine detection in cement with laser-induced breakdown spectroscopy in the infrared and ultraviolet spectral range”, *Spectrochim. Acta Part B* 64 (2009) 1135–1140.
 24. G. Wilsch, F. Weritz, D. Schaurich and H. Wiggenhauser, “Determination of chloride content in concrete structures with laser-induced breakdown spectroscopy”, *Construction and Building Materials* 19, 724–730 (2005).
 25. S. Hong, W. Wai-Lok Lai, G. Wilsch, R. Helmerich, R. Helmerich, T. Günther and H. Wiggenhauser, “Periodic mapping of reinforcement corrosion in intrusive chloride contaminated concrete with Ground Penetrating Radar (GPR)”, *Construction and Building Materials* 66, 671–684 (2014).
 26. U. Angst, B. Elsener, C.K. Larsen and Ø. Vennesland, “Critical chloride content in reinforced concrete — A review”, *Cement and Concrete Research* 39, 1122–1138 (2009).
 27. W. Chesner and N.J. McMillan, “Laser Spectroscopy for Rapid Profiling of Steel Bridge Coating, Corrosion, and Heavy Metals”, *Final Report for Highway IDEA Project 164*, September 2014.
 28. S. Kaski, H. Hakkanen and J. Korppi-Tommola, “Determination of Cl/C and Br/C ratios in pure organic solids using laser-induced plasma spectroscopy in near vacuum ultraviolet”, *J. Anal. At. Spectrom.*, 19, 474-478 (2004).
 29. N. Idris, T. Kobayashi, M.M. Suliyanti, H. Kurniawan, T. Jie Lie, K. Kagawa and Y. I. Lee, “Confinement Effect in TEA CO₂ Laser-Induced Plasma on Solid Organic Samples”, *Journal of the Korean Physical Society*, 47(2), 256-262 (2005).
 30. M.S. Dimitrijevic and S. Sahal-Bréchet, “Stark broadening of Ca II spectral lines”, *J. Quant. Spectrosc. Radiat. Transfer*, 49(2), 157-164 (1993).
 31. J. Vogelgesang and J. Hädrich, “Limits of detection, identification and determination: a statistical approach for practitioners”, *Accred. Qual. Assur.*, 3, 242-255 (1998).
 32. J. M. Mermet, “Calibration in at. spect.: A tutorial review dealing with quality criteria,

- weighting procedures and possible curvatures”, *Spectrochim. Acta B*, **65**, 509 (2010).
33. P.W.J.M. Boumans, “Measuring detection limits in inductively coupled plasma emissionspectrometry using the “SBR-RSDB approach”-1. A tutorial discussion of the theory”, *Spectrochim. Acta Part B*, **46**, 431 (1991).
 34. M. Carré, S. Excoffier and J.M. Mermet, “A study of the relation between the limit of detection and the limit of quantitation in ICP spectrochemistry”, *Spectrochim. Acta Part B*, **52**, 2043 (1997).
 35. E. Voigtman, “Limits of detection and decision. Part 1-4”, *Spectrochim. Acta Part B*, **63**, 115-165 (2008).
 36. J.M. Mermet, “Limit of quantitation in atomic spectrometry: An unambiguous concept?” *Spectrochim. Acta Part B*, **63**, 166 (2008).
 37. J.M. Mermet, P. Mauchien and J-L. Lacour, “Processing of shot-to-shot data to improve precision in LIBS”, *Spectrochim. Acta Part B*, **63**, 999 (2008).
 38. E. Poussel and J-M. Mermet, “Simultaneous measurements of signal and background in ICP-AES: effects on precision, limit of detection and limit of quantitation”, *Spectrochim. Acta, Part B*, **51**, 75 (1996).
 39. K. Danzer, “Comparison of sampling procedures for investigation of chemical homogeneity of solids by spark emission spectrography”, *Spectrochim. Acta* , **39B**, 949 (1984).
 40. L. Kempenaers, L. Vincze and K. Janssens, “The use of synchrotron micro-XRF for characterization of the micro-heterogeneity of heavy metals in low-Z reference materials”, *Spectrochim. Acta Part B*, **55**, 651 (2000).
 41. F.R. Doucet, P.J. Faustino, M. Sabsabi, and R.C. Lyon, “Quantitative molecular analysis with molecular bands emission using laser-induced breakdown spectroscopy and chemometrics”, *J. Anal. At. Spectrom.*, **23**, 694–701(2008).
 42. A.A. Bol'shakov, X. Mao, J.J. Gonzalez and R.E. Russo, “Laser Ablation Molecular Isotopic Spectrometry: current state of the art”, *J. Anal. At. Spectrom.*, **31**, 119 (2016).
 43. U.Heitmann, H. Becker-Ross, S. Florek, M.D. Huang and M. Okruss, “Determination of non-metals via molecular absorption using high-resolution continuum source absorption spectrometry and graphite furnace atomization”, *J. Anal. At. Spectrom.*, **21**, 1314–1320 (2006).
 44. M.D. Huang, H. Becker-Ross, S. Florek, U. Heitmann, M. Okruss, “Determination of halogens via molecules in the air–acetylene flame using high-resolution continuum source absorption spectrometry, Part II: Chlorine”, *Spectrochim. Acta Part B* **61**, 959–964 (2006).
 45. M. Fechetia, A.L. Tognon, M.A.M.S. da Veiga, “Determination of chlorine in food samples via the AlCl molecule using high-resolution continuum source molecular absorption spectrometry in a graphite furnace”, *Spectrochim. Acta Part B*, **71-72**, 98–101 (2012).
 46. É.R. Pereira, B. Welz, A.H.D. Lopez, J.S. de Gois, G.F. Caramori, D.L.G. Borges, E. Carasek, J.B. de Andrade, “Strontium mono-chloride — A new molecule for the determination of chlorine using high-resolution graphite furnace molecular absorption spectrometry and direct solid sample analysis”, *Spectrochim. Acta Part B*, **102**, 1–6 (2014).
 47. M. Gaft, L. Nagli, N. Eliezer, Y. Groisman and O. Forni, “Elemental analysis of halogens using molecular emission by LIBS in air”, *Spectrochim. Acta Part B*, **98**, 39-47 (2014).

48. C. Álvarez, J. Pisonero, N. Bordel, “Quantification of fluorite mass-content in powdered ores using a Laser-Induced Breakdown Spectroscopy method based on the detection of minor elements and CaF molecular bands”, *Spectrochimica Acta Part B*, 100, 123–128 (2014).
49. O. Forni, M. Gaft, M. Toplis, S.M. Clegg, S.Maurice, R.C. Wiens, N. Mangold, V. Sautter, O. Gasnault, G. Berger, M. Nachon, P.-Y. Meslin, D. Blaney, A. Cousin, “First fluorine and chlorine detection with CHEMCAM on board MSL”, *Eight Int. Conf. on Mars*, 1062 (2014).
50. T. Guenther, R. Glaus, G. Wilsch and I. Gornushkin, “Detection of CaCl in cement by LIBS”, Poster presentation at the *8th Euro-Mediterranean Symposium on Laser Induced Breakdown Spectroscopy (EMSLIBS 2015)*, Linz, Austria, 14-18 September 2015.
51. W.B. Jones, E. Ewusi-Annan, T. Guenther, B.W. Smith and N. Omenetto, “Atomic and molecular LIBS for the detection of chlorine in concrete”, Poster Presented at *Pittcon 2016*, Atlanta, GA (USA), March 2016.
52. A.E. Parker, Band Systems of MgCl, CaCl and SrCl, *Phys. Rev.*, 47, 349-358 (1935). R.K. Asundi, “The band systems and structure of CaCl”, *Proc. Indian Acad. Sci*, 830-841 (1935).
53. L.E. Berg, L. Klynning and H. Martin, “Laser spectroscopic investigations of CaCl. II. Rotational analysis of the B(σ)-X(Σ) Transitions”, *Physica Scripta*, 22, 216-220 (1980).
54. A. Pereira, “Analysis of the ultraviolet C (Π)-X (Σ) Band System of CaCl”, *Physica Scripta*, 34, 788-796 (1986).
55. P.J. Domaille, T.C. Steimle, N.B. Wong and D.O. Harris, “High-Resolution Laser excitation spectroscopy: Analysis of the B-X system of CaCl”, *J. Mol. Spectrosc.*, 65, 354-365 (1977).
56. P.Y. Virmani, H.Ghasemi, *Literature review of chloride threshold values for grouted post-tensioned tendons*, Summary Report No. FHWA-HRT-12-067, November 2012 <http://fhwa.dot.gov/research/>
57. A. Taffe, D. Schaurich, G. Wilsch and F. Weritz, “Development of a portable LIBS-device for quality assurance in concrete repair”, in *Concrete Repair, Rehabilitation and Retrofitting II* – Alexander et al, Eds., Taylor and Francis Group, London (2009) ISBN 978-0-415-46850-3.
58. S. Millar, C. Gottlieb, G. Wilsch, T. Eichler, C. Bohling and A. Molkenhuth, *International Symposium Non-destructive Testing in Civil Engineering (NDT-CE)*, BAM, Berlin (Germany), 15-17 September 2015. (www.ndt.net/?id=18296).
59. S. Eto and T. Fujii, “Laser-induced Breakdown Spectroscopy system for remote measurement of salt in a narrow gap”, *Spectrochim. Acta Part B*, 116, 51-57 (2016).
60. C. Monticelli, M.E. Natali, A. Balbo, C. Chiavari, F. Zanotto, S. Manzi and M.C. Bignozzi, “Corrosion behavior of steel in alkali-activated fly ash mortars in the light of their microstructural, mechanical and chemical characterization”, *Cement and Concrete Research*, 80, 60-68 (2016).
61. B. Šavijia, E. Schlangen, J. Pacheco, S. Millar, T. Eichler and G. Wisch, *J. Adv. Concrete Technology*, 12, 425-442 (2014).
62. S. Eto, T. Matsuo, T. Matsumura, T. Fujii and M.Y. Tanaka, “Quantitative estimation of carbonation and chloride penetration in reinforced concrete by laser-induced breakdown spectroscopy”, *Spectrochim. Acta Part B*, 101, 245-253 (2014).

63. S. Eto, J. Tani, K. Shirai and T. Fujii, "Measurement of concentration of chlorine attached to a stainless steel canister material using laser-induced breakdown spectroscopy", *Spectrochim. Acta Part B*, 87, 74-80 (2013).
64. N. Silva, "Chloride Induced Corrosion of Reinforcement Steel in Concrete -Threshold Values and Ion Distributions at the Concrete-Steel Interface", PhD Dissertation, (Doktorsavhandlingar vid Chalmers tekniska högskola Ny serie nr 3489 ISSN 0346-718X), Chalmers University of Technology, Gothenburg, Sweden (2013).
65. M. Torres-Luque, E. Bastidas-Arteaga, F. Schoefs, M. Sanchez-Silva and J.F. Osmá. "Non-destructive methods for measuring chloride ingress into concrete: State-of-the-art and future challenges", *Construction and Building Materials*, 68, 68-81 (2014).
66. K.D. Stanish, R.D. Hooton and M.D.A. Thomas, "Testing the Chloride Penetration Resistance of Concrete: A Literature Review", Department of Civil Engineering, University of Toronto, Toronto, Ontario, Canada. (FHWA Contract DTFH61-97-R-00022 "Prediction of Chloride Penetration in Concrete").